CHALMERS
UNIVERSITY OF TECHNOLOGY

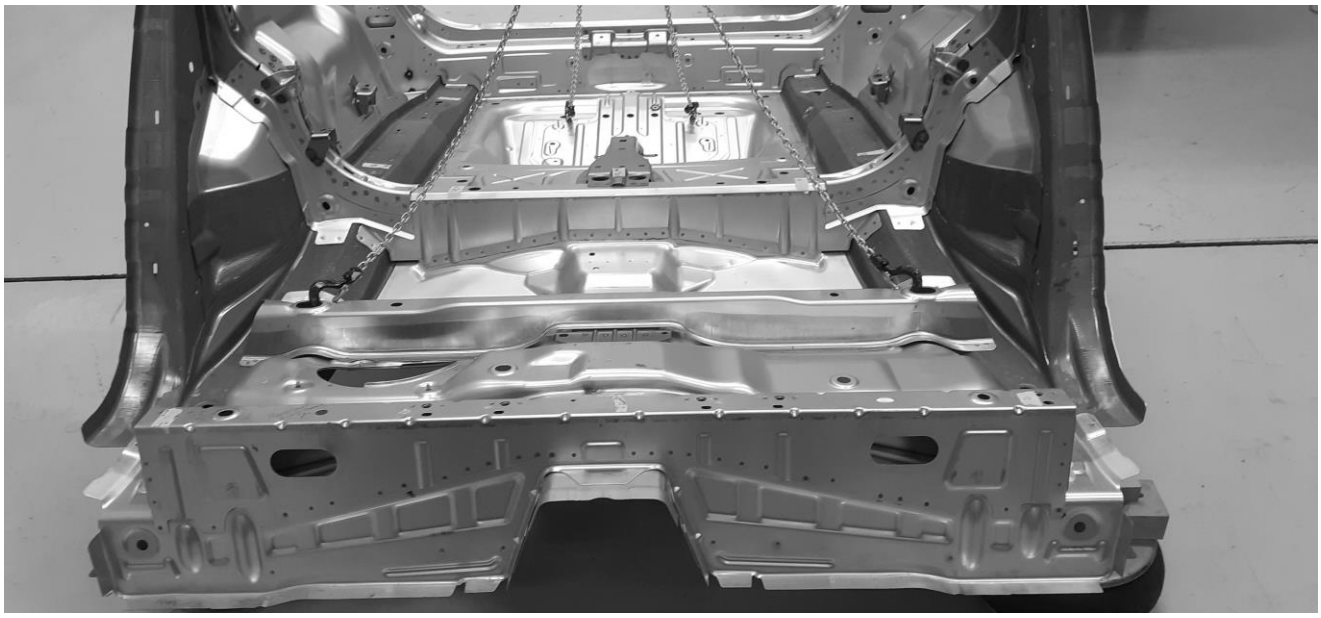

Sub-Assemblies Correlation of a BIW Architecture

Global Modes and Main Transfer Functions

Master's thesis in Applied Mechanics

Wilhelm Sjödin

DEPARTMENT OF MECHANICS AND MARITIME SCIENCES
CHALMERS UNIVERSITY OF TECHNOLOGY

Gothenburg, Sweden 2022
www.chalmers.se

MASTER'S THESIS IN APPLIED MECHANICS

Sub-Assemblies Correlation of a BIW Architecture

Global Modes and Main Transfer Functions

Wilhelm Sjödin

CHALMERS
UNIVERSITY OF TECHNOLOGY

Department of Mechanics and Maritime Sciences
Division of Dynamics
Chalmers University of Technology
Gothenburg, Sweden 2022

Sub-Assemblies Correlation of a BIW Architecture
Global Modes and Main Transfer Functions

WILHELM SJÖDIN

Supervisor: Álvaro Valencia Ruiz, Senior CAE Engineer, Personal Centre, Volvo Car Corporation

Examiner: Thomas Abrahamsson, Full Professor, Mechanics and Maritime Sciences, Division of Dynamics, Chalmers

Master's thesis 2022:09
Department of Mechanics and Maritime Sciences
Division of Dynamics
Chalmers University of Technology
SE-412 96 Gothenburg
Sweden
Telephone: +47 (0)31-772 1000

Cover:
The picture shows one of the sub-assemblies of a Body in White, the Floor Rear, located in the NVH laboratory at Volvo Car Corporation.

Department of Mechanics and Maritime Sciences
Gothenburg, Sweden 2022

Abstract

This dissertation focuses on correlation between measurement and simulation results on a Body in White (BIW). The purpose is to set up and evaluate a correlation methodology, where each sub-assembly of the car body is assessed separately to be able to localize the finite element model uncertainties. The sub-assemblies correlated in this dissertation are the Floor Rear and the Body Side Outer, of a BIW architecture. To obtain the dynamic properties of the car body, several experimental and CAE based methods are employed and evaluated.

The sub-assemblies of a car body are usually connected using different joining methods, such as spot welds and adhesives. The first step is to set up two FE-models of the sub-systems, from CAD-geometries and a complete FE-model of the BIW. This is done by using ANSA as a pre-processor. Normal modes analysis (NMA) and modal frequency response analysis (MFRA) can then be utilized in MSC NASTRAN to calculate mode shapes, resonance frequencies and transfer functions. These numerical results are then used in a pre-test analysis to decide accelerometer and impact locations for the experimental modal analysis (EMA). Thus, qualitative measurement data can be obtained, capturing the dynamical behavior of the structure. Measurements are then done using an impact hammer, triaxial accelerometers, and measurement software and hardware from Müller-BBM VibroAkustik Systeme (PAK), as well as from Siemens (LMS Testlab).

The correlation of the sub-assemblies focuses on physical differences between the FE-model and the manufactured parts. Uncertainties identified are the adhesives, welds, structural damping, and the thickness distributions. To quantify differences between measurement data and simulation data, and to study the sensitivity of different properties, transfer functions are analyzed. Global modes and resonance frequencies are either identified from real and imaginary parts of the transfer functions, or from experimental and analytical modal analysis.

The first conclusion drawn was that when correlating sub-assemblies, the FE-model must be adapted to the current step in the manufacturing process. One example is the adhesives that are cured at a later stage in the factory, and thus the ultimate material properties cannot be applied directly using the methodology presented in this dissertation. Furthermore, conclusions on the influence of the welds, structural damping, the thickness distribution and the mass is presented in this dissertation.

By correlating the car body piecewise, the sensitivities and uncertainties were localized, and could thus be analyzed in more detail. Furthermore, once the complete body is assembled the only uncertainties lies in the connections between the sub-assemblies, and not in the different sub-systems themselves. The presented methodology can thus be considered more robust than by correlating the complete body directly.

Sammanfattning

Denna masteruppsats fokuserar på korrelation mellan simuleringar och mätdata av en bilkaross. Syftet är att utveckla och utvärdera en korrelationmetod där olika delsystem av bilens kaross utvärderas separat, för att kunna lokalisera osäkerheter i en finit elementmodell av karossen. De delsystem som behandlas i denna avhandling är yttre sidoparti och bakre golvparti. För att bestämma strukturens dynamiska egenskaper används ett flertal olika, experimentella och beräkningsbaserade metoder.

Karossen är sammansatt av ett antal olika delar, såsom formpressade stålplåtar vilka är sammanfogade med exempelvis punktsvets eller lim. Första steget i denna avhandling är att, utifrån CAD-modeller och en komplett finit elementmodell av karossen, ta fram två finit elementmodeller av bakre golvpartiet och yttre sidopartiet. Till detta används ANSA som pre-processor.

Efterföljande steg är att utföra egenmodsanlys och frekvensresponsanalys i MSC NASTRAN, för beräkning av resonansfrekvenser, modformer och överföringsfunktioner. Dessa numeriska resultat används sedan i en förtestsanalys för att bestämma accelerometerpositioner och excitationspunkter för kvalitativa mätdata som väl fångar upp strukturens dynamiska egenskaper. Mätningarna genomförs därefter med treaxliga accelerometrar, impulshammare och mätsystem från Müller-BBM VibroAkustik Systeme (PAK) såväl som från Siemens (LMS Testlab).

Korrelationen av karossen fokuserar i denna uppsats på fysiska olikheter mellan finit elementmodellerna och de tillverkade delarna. Osäkerheter som identifierats hör till modelleringen av lim, svetsar, strukturell dämpning och distributionen av tjocklek efter metallformning. För att kvantifiera olikheter mellan beräkningsdata och mätdata, samt bestämma känsligheten i olika parametrar, analyseras överföringsfunktioner. Globala moder och resonansfrekvenser identifierades antingen direkt från överföringsfunktioner, eller från experimentell och analytisk modalanalys.

En första slutsats som drogs var att korrelationen av delsystem kräver vissa åtgärder angående från vilket steg i tillverkningen karosseridelarna hämtas. Ett tydligt exempel är att limmet inte härdat på sidopartiet eller golvpartiet, och därav kan inte de slutgiltiga materialegenskaperna användas i finit elementmodellen. Ytterligare har flera andra slutsatser presenterats i rapporten gällande påverkan från svetsar, modellering av dämpning och tjockleksvariationer.

Genom att korrelera karossen stegvis kunde känsligheten av parametrar analyseras noggrannare, samtidigt som modellosäkerheter kunde lokaliseras. När delsystemen sedan sammanfogas till den kompletta karossen, kan således osäkerheter skalas ned till de element som finns mellan de olika delsystemen. Den presenterade metoden bedöms därför vara robust och tillförlitlig.

Preface

This Master's thesis is within the field of experimental NVH and computational structural dynamics and has been conducted at Personal Centre (previously NVH Center) at Volvo Car Corporation. The duration of this thesis has been 20 weeks, during the spring term of 2022, and comprises 30 credits. The purpose of the master's thesis has been to set up the basis of a robust process of correlation for a Body in White, considering the sub-assemblies which are part of the BIW.

A special thanks to my supervisor and many other team members at Volvo Car Corporation for many interesting discussions regarding CAE, automotive engineering and much more. I would also like to take the opportunity to thank my examiner who taught me the theory behind this topic in Structural Dynamics and FE-model validation courses at Chalmers.

Álvaro Valencia Ruiz has been my supervisor throughout this project, with a long experience within the field of NVH, both from testing and CAE, I could not hope for a better person to guide me. His enthusiasm to teach, and to also embrace new ideas made this project a worthwhile experience for both of us.

Contents

List of Figures

List of Tables

1. Introduction

Validation of finite element models used for computational structural dynamics is an important task. With a validated model, results from analysis can be trusted and it is ensured that physical results are obtained. By performing NVH-measurements, frequencies and mode shapes can be identified and compared to those from analysis. At the same time the damping can be decided from these measurements, and then be implemented in FEA. Such a correlation task has been performed in this dissertation, studying differences between FEA and testing. When satisfactory results are achieved, the finite element model can be viewed as validated for its intended purposes.

1.1 Background

The Body in White (BIW) is the frame of the car, where different structures have been joined together. For the body it is important that several requirements are fulfilled. Important properties relate to static stiffness, passive safety, and to protect occupants from unwanted noise, vibrations, and harshness (NVH). At BIW-level no trim items or closures such as the doors are added, neither the chassis nor the driveline etcetera is implemented at this stage of the manufacturing.

Different sub-assemblies can be considered to build up the BIW, such as the front structures, rear structures, top-hat etcetera. Different joining methods are then used, some of which are welding and using adhesives. In finite element modelling these are often a source of non-linearities. The sub-assemblies considered in this thesis are the Floor Rear and the Body Side Outer, presented in Figure 1.1.

Figure 1.1. *Floor Rear (left) and Body Side Outer (right).*

To obtain dynamic properties of the BIW two main methods have been utilized in this project, experimental methods and analytical methods. Using measurement data, experimental modal analysis (EMA) and a direct approach using FRFs have been performed. In simulation, normal modes analysis (NMA) and modal frequency response analysis (MFRA) have been employed.

1.2 Target & limitations

The purpose of this master's thesis is to set up and evaluate a process of robust correlation at BIW level by individually correlating the sub-assemblies of the BIW. The sub-assemblies studied in this report are the Floor Rear and the Body Side Outer.

Pre-test planning, instrumenting, and performing measurements, as well as simulations and correlation are within the scope of this project, which ensures that similar set-ups can be studied in the correlation phase of the project.

By individually correlating the sub-assemblies, uncertainties at BIW level can be isolated and thus more easily be found than by studying the complete structure directly. When correlating the complete BIW the uncertainties are thus limited to the connections, connecting the sub-assemblies together.

Due to the limitation of time in this project, the complete correlation procedure could not be evaluated and developed. For example, all sub-assemblies have not been considered even though the same procedure is applicable on both sub-assemblies as well as the complete BIW. Another parameter that was not studied was the effect on dynamical properties due to the surface treatments, such as electro coating. The complete correlation procedure is presented in Figure 1.2, where it is also seen in which area this thesis is conducted.

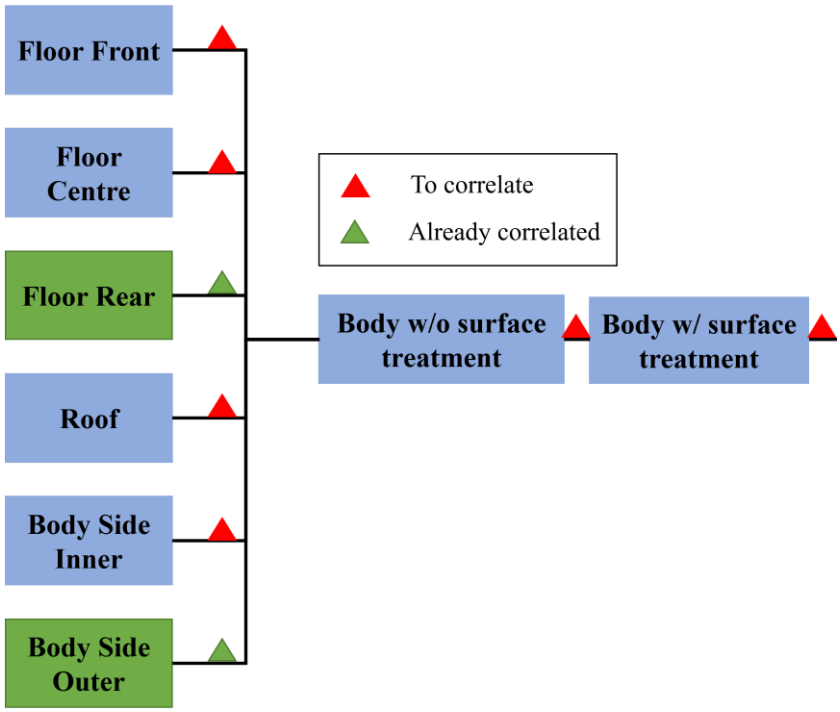

Figure 1.2. *Correlation procedure, where green shows objects within the scope of this thesis.*

2. Theory

Below the relevant theory needed for this project is presented. For basic understanding of the finite element method please see Introduction to the finite element method (Ottosen & Petersson, 1992), and for further reading on the theory behind computational and experimental modal analysis please see Fundamentals of structural dynamics (Craig, 2011). First the engineering and mathematical model for a single degree of freedom will be presented, and some of its dynamics.

2.1 Engineering and mathematical model

The engineering model of a one degree of freedom system is seen in Figure 2.1. Where a cart is representing a lumped mass (m) moving in x-direction without friction. A spring (stiffness k) and a damper (damping coefficient c) are connecting the cart to a rigid wall, and there is a horizontal time dependent force ($F(t)$) acting on the system.

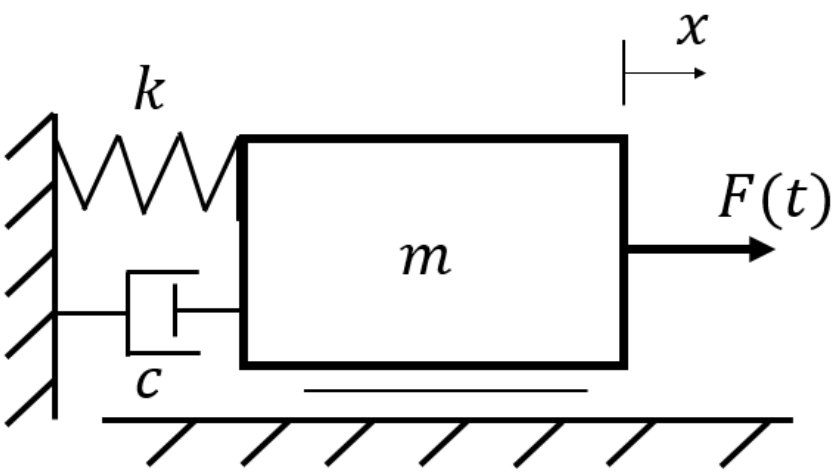

Figure 2.1. *Engineering model of single degree of freedom system.*

The mathematical model of this system is then described by the structural dynamics equation (SDE):

$$m\ddot{x} + c\dot{x} + kx = F(t) \tag{2.1}$$

Fourier's harmonic assumption states that the response shares the same harmonic behavior as the stationary harmonic force (Abrahamsson, 2000). The mathematical representation of this force with angular frequency ω and amplitude $\hat{f}$ and the corresponding response is:

$$F(t) = \hat{f}e^{i\omega t} \tag{2.2}$$

$$x = \hat{x}e^{i\omega t} \tag{2.3}$$

The SDE together with the harmonic assumption then becomes:

$$\frac{\hat{x}}{\hat{f}} = \frac{1}{(k - \omega^2 m) + i\omega c} \tag{2.4}$$

The angular frequency and damping factor of the system are defined as follows:

$$\omega_0 = \sqrt{\frac{k}{m}} \tag{2.5}$$

$$\xi = \frac{c}{2\sqrt{km}} \tag{2.6}$$

The receptance, describing the response obtained by the excitation on the system, with one degree of freedom is then:

$$\frac{\hat{x}}{\hat{f}} = \frac{1/k}{\left(\left(1 - \left(\frac{\omega}{\omega_0}\right)^2\right) + 2\xi\frac{\omega}{\omega_0}i\right)} \tag{2.7}$$

With corresponding derivatives for mobility and inertance:

$$\frac{\hat{\dot{x}}}{\hat{f}} = \frac{1}{k}\frac{i\omega}{\left(\left(1 - \left(\frac{\omega}{\omega_0}\right)^2\right) + 2\xi\frac{\omega}{\omega_0}i\right)} \tag{2.8}$$

$$\frac{\hat{\ddot{x}}}{\hat{f}} = \frac{1}{k}\frac{-\omega^2}{\left(\left(1 - \left(\frac{\omega}{\omega_0}\right)^2\right) + 2\xi\frac{\omega}{\omega_0}i\right)} \tag{2.9}$$

These transfer functions can be divided into real and imaginary parts. For the inertance this becomes:

$$Re\left(\frac{\hat{\ddot{x}}}{\hat{f}}\right) = \frac{-\frac{1}{k}\left(1 - \left(\frac{\omega}{\omega_0}\right)^2\right)\omega^2}{\left(1 - \left(\frac{\omega}{\omega_0}\right)^2\right)^2 + \left(2\xi\frac{\omega}{\omega_0}\right)^2} \tag{2.10}$$

$$Im\left(\frac{\hat{\ddot{x}}}{\hat{f}}\right) = \frac{\frac{1}{k}\left(2\xi\left(\frac{\omega}{\omega_0}\right)\right)\omega^2}{\left(1 - \left(\frac{\omega}{\omega_0}\right)^2\right)^2 + \left(2\xi\frac{\omega}{\omega_0}\right)^2} \tag{2.11}$$

It is then of special interest to study how these behave at the natural angular frequency ω_0:

$$Re\left(\frac{\hat{\ddot{x}}}{\hat{f}}\right)\Big|_{\omega=\omega_0} = 0 \tag{2.12}$$

$$\frac{d}{d\omega}\left(Im\left(\frac{\hat{\ddot{x}}}{\hat{f}}\right)\right)\Big|_{\omega=\omega_0} = \frac{\omega_0}{2k\xi} \approx 0 \tag{2.13}$$

It is then seen that when the forcing function is at the angular frequency, $\omega = \omega_0$, a maximum or minimum is expected when studying the imaginary part of the inertance. For the real part of the inertance the transfer function is expected to cut the x-axis. This holds true for the inertance obtained both from simulation and vibration testing, for one degree of freedom. These results are useful when identifying modes, and distinguishing modes from one another directly from measured data.

2.2 Testing and NVH-analysis

One method of experimentally determining the dynamical properties of a structure is called experimental modal analysis (EMA). A simple setup of a vibration test is seen in Figure 2.2. Here a plate is being tested by applying a force in one corner and measuring the response in the opposite corner. The plate is being tested in close to free-free conditions, by suspending it with bungee cords to a rigid wall. Both the force and response are being measured.

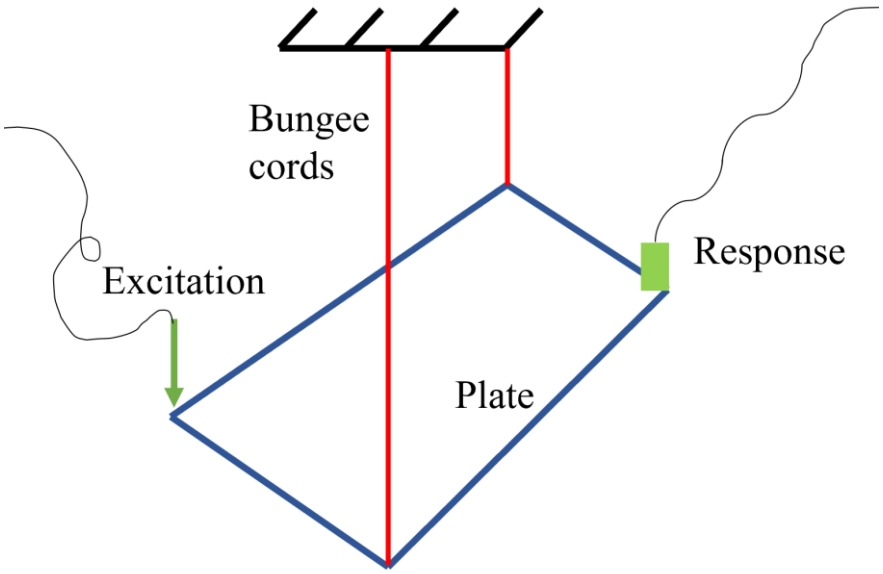

Figure 2.2. *Sketch of a vibration testing setup.*

Using this setup, a frequency response function can be obtained as the ratio between the output response due to the applied force. The time domain data is transformed to the frequency domain

using Fast Fourier Transform, for more reading on signal processing see for example Signal Processing (Mohanty, 1987).

2.2.1 Direct approach for estimating mode shapes

Due to damping, the response can then be viewed in either magnitude and phase form or by the real and imaginary parts. By studying the peak amplitudes of the imaginary parts of the FRF, the approximate mode shapes can be estimated directly from the measured data (Avitabile, 2001). This approach can be implemented in a script extracting data from measurements and simulations, which allows for quick iterations during correlation between test and CAE.

A physical interpretation of the imaginary part is thus that it gives information about the mode shape. In contrast the amplitude is always positive and does not give such information. Together with the mathematical model of a single degree of freedom system, it has been shown that the imaginary part should have either a maximum or minimum at a natural frequency. Whilst the real part should cut the x-axis. For a simple beam, the mode shape has been roughly estimated from the peak amplitudes of the imaginary parts of FRFs at three different measurement points, as done in Figure 2.3. In the figure, the three different boxes represent three different responses after excitation.

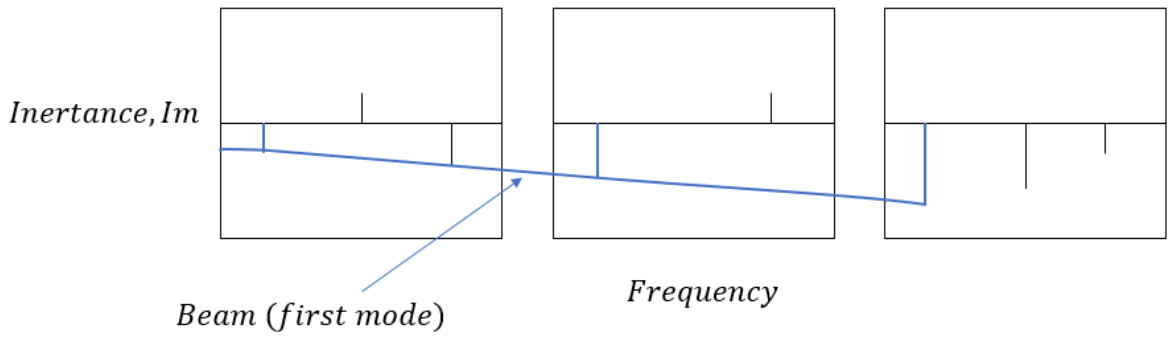

Figure 2.3. *Rough estimation of mode shape using imaginary part of inertance, illustration on beam.*

2.2.2 Experimental modal analysis and system identification

When performing a modal analysis, the parameters characterizing the dynamic behavior of a structure are obtained. In CAE, a NMA can be submitted for the chosen model, in for example MSC NASTRAN. In testing some sort of system identification is necessary once the vibration test has been performed.

Several frequency response functions from measurements are then used as input to deduce the system poles. One approach is the PolyMAX method, based on a least-squares curve fitting approach. This method is currently implemented in LMS Testlab (Siemens, 2022). For further

reading on the development and use of this method, please see for example *Automotive and aerospace applications of the PolyMAX modal parameter estimation method* (Peeters et al., 2004).
Using the system identification in Testlab, the modes found during testing of the structure can be effectively displayed in a stabilization diagram over a specified frequency band. It graphically shows the poles/modes of the structure and ranks them in several categories as described in the methodology, such as a stable pole fulfilling all chosen criteria. The poles can then be automatically or manually selected, and a further calculation can be made using the identified model. In this way mode shapes, resonance frequencies and damping factors are obtained from a curve fitted model.

An overview of the method is seen in Figure 2.4, where a test has been performed on an outer side of a car body. The test results in FRFs can then be used for curve fitting, from which resonance frequency, damping and mode shapes can be obtained as described by Avitabile (2001).

In Figure 2.4, the frequency response function (FRF) between degree of freedom i and degree of freedom j is written as, $h_{ij}(i\omega)$. N is the number of modes contributing to the response in the chosen frequency range, r_{ijk} is the residue value for mode k. Furthermore, λ_k is the pole value for mode k and asterisk labels complex conjugates.

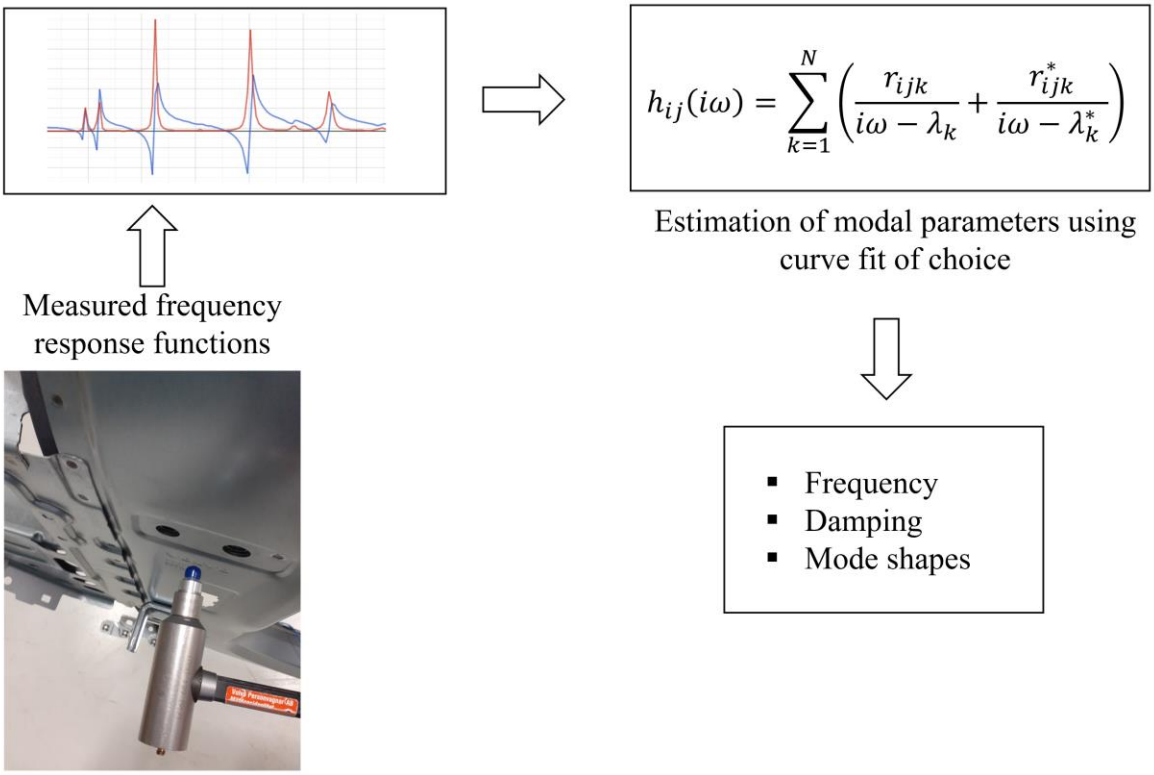

Figure 2.4. *Overview of curve fitting to estimate modal parameters (EMA).*

2.2.3 Direct approach for calculating damping

In FEA a common uncertainty is the damping and to reduce this uncertainty the FRF obtained from vibration testing can be utilized to calibrate the model directly, without using system identification. There are different damping quantities that can be used, such as the damping factor Q. Methods such as the Three dB Method can be employed to calculate the damping factor using experimental data. In this project NVH measuring software PAK (Müller-BBM VibroAkustik Systeme GmbH, 2022) was used to calculate the damping factor directly from measured FRFs. The damping factor can be obtained according to:

$$Q = \frac{f_0}{f_2 - f_1} \tag{2.14}$$

The damping is frequency dependent and different techniques to apply the damping can be utilized. In this project a modal damping was applied on the specific modes. Please see Figure 2.5 for an overview of the above quantities in a graphical illustration of test data. Since the damping is calculated on a set of test data at a certain frequency, it is understood that the damping must be decided for a specific structure and is not a general quantity for all sub-assemblies of the car body.

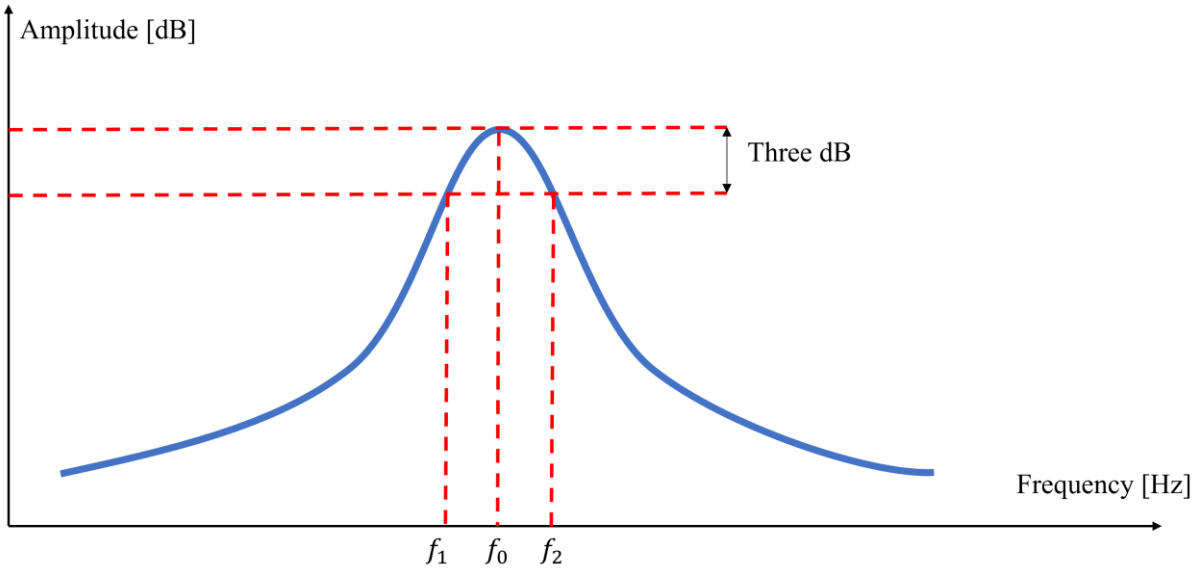

Figure 2.5. *Three dB Method for calculating damping from an experimentally obtained FRF.*

2.3 Modal assurance criterion and correlation

There are several different eigenvector correlation metrices that can be utilized together with modal parameters of the structure during correlation using experimental and simulation data. The one used in this report is the Modal Assurance Criterion (MAC), which ideally should be one if the experimental and simulation eigenvectors are co-linear. The MAC number is obtained by:

$$MAC(i,j) = \frac{\left(\boldsymbol{\phi}_{iX}^{T}\boldsymbol{\phi}_{jA}\right)^{2}}{\|\boldsymbol{\phi}_{iX}\|_2^{\,2}\left\|\boldsymbol{\phi}_{jA}\right\|_2^{\,2}} \tag{2.15}$$

Since in vibration testing not all degrees of freedom can be captured, the eigenvectors in the modal matrix, $\boldsymbol{\Phi}_A$, must be selected from simulation at locations where the responses are obtained in testing. The corresponding modal matrix from testing is $\boldsymbol{\Phi}_X$. Co-linear eigenvectors thus give a MAC-number of one, and orthogonal eigenvectors give a MAC-number of zero.

Furthermore, when comparing data from testing and simulation, eigenvalues should be close or ideally the same. Also, the frequency response functions should ideally give similar and overlapping curves when plotted against each other. Parallel to using MAC-numbers for validation, the mode shapes can be compared visually between testing and simulation. For this EMA can be helpful, since the FE-model and curve fitted model can be plotted next to each other using PLOTEL elements as seen in Figure 2.6.

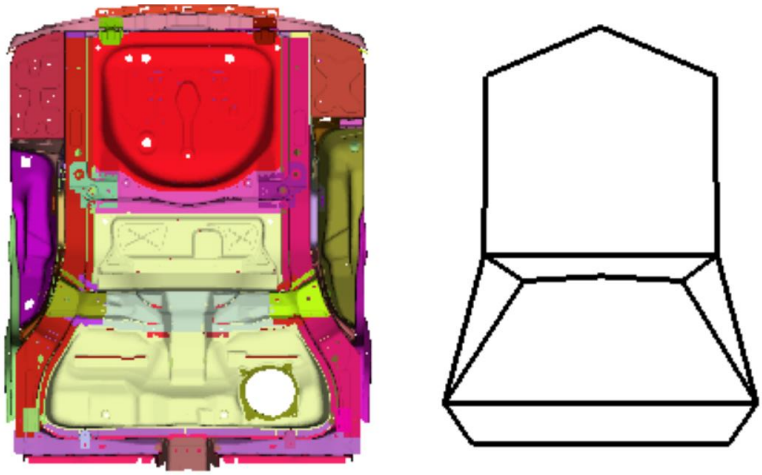

Figure 2.6. *Curve fitted model from measurements (right), next to FE-model (left) when correlating mode shapes in META.*

2.4 Metal forming and stamping simulation

To manufacture certain components of the BIW, sheet metal forming is used. Applying forces causing the material to deform can generate complex shapes as described by Hågeryd et al. (2016). After a stamping process the sheet metal thickness varies and is not uniform, this data can be obtained by using stamping simulations (Böttcher & Frik, 2003). It has been shown that a mapped thickness distribution affects the dynamical properties of the structure (Eppler & Schatz, 2007). Thus, considering the varying thickness is of importance when comparing numerical results with experimental results. Results from a stamping simulation performed at VCC can be seen in Figure 2.7 (a) for a part of a side member and (b) on a lower inner C-pillar.

It is important to notice that the mesh is different from forming simulations compared to the requirements for NVH-simulations, these parts can thus not be implemented directly, and ANSA is used to for mapping the results to the chosen mesh by specifying a search distance.

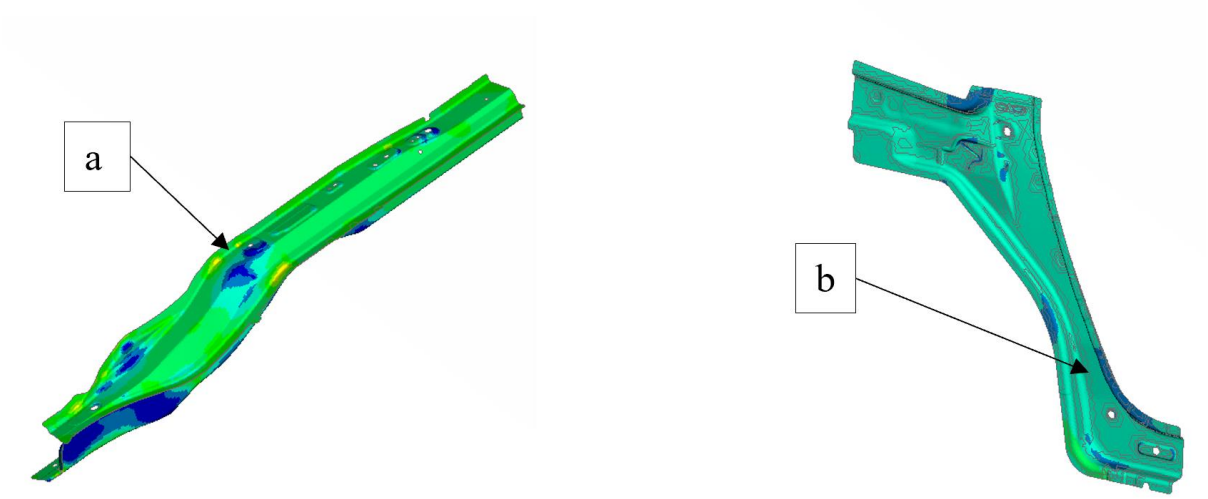

Figure 2.7. *Varying thickness from stamping simulation. (a) Darker blue shows a thinning area on one of the side members and (b) thinning area on the lower inner C-pillar.*

3. Method

In this chapter the methodology of this dissertation is described, together with the FE-model necessary to set up certain simulations. Two main simulation procedures have been employed, normal modes analysis (NMA) and modal frequency response analysis (MFRF). Vibration testing was employed to obtain experimental results, using e.g., triaxial accelerometers and an impact hammer. Different methods of identifying modes have been employed on both experimental and numerical results for correlation purposes. The model has been prepared mostly using the pre-processor ANSA, for example meshing and mapping simulation results. Post-processing has been performed on both simulation and experimental data, using META and HyperGraph (Altair, 2022) for simulations, and PAK and Simcenter LMS Testlab for experimental data.

3.1 FE-model groundwork

In the following sections the FE-model will be described and compared to the manufactured parts. Steps and tools used to obtain the model used in simulations will be described in some detail.

3.1.1 Floor Rear and Body Side Outer

The CAD-models of the outer side and the rear floor of the body are seen to the left in Figure 3.1, these assemblies consist of several parts connected with different joining methods such as bolts. CAD data was used when setting up the finite element models, together with a complete finite element model of the BIW, developed by engineers at VCC. Using the CAD data, parts could be identified that could be transferred to separate includes in ANSA. Using Boolean and connection tools in the pre-processor, different parts could be separated and joined together depending on the studied assembly. Thus, two separate models were obtained from the complete model.

Furthermore, some parts were introduced to match the version of the car obtained from the production plant. In Figure 3.2 (a) the initial version of the FE-model is seen, and in (b) the introduced panel is seen after visual inspection of the manufactured floor. For these parts, mid-surfaces of the CAD were extracted and later a shell mesh was created on the mid-surface. To ensure the mesh quality criteria were fulfilled for NVH purposes, mesh-tools provided in the pre-processor were employed until the quality criteria were satisfied indicated by black color in the zoomed in area in Figure 3.2.

For correlation purposes it is of course important that the model represents the physical parts, thus visual inspection of the physical parts is critical. As seen from the manufactured parts in Figure 3.3, the introduced version seen in Figure 3.2 now represents the geometry better.

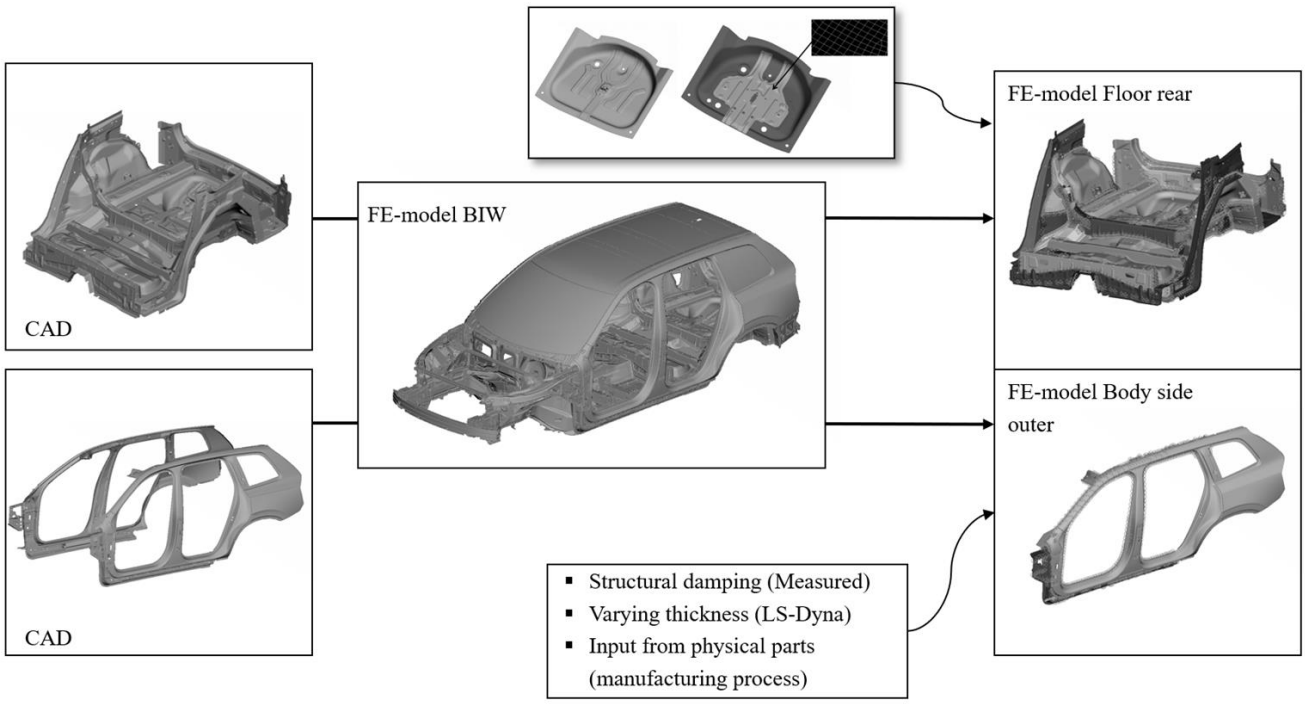

Figure 3.1. *FE-model groundwork.*

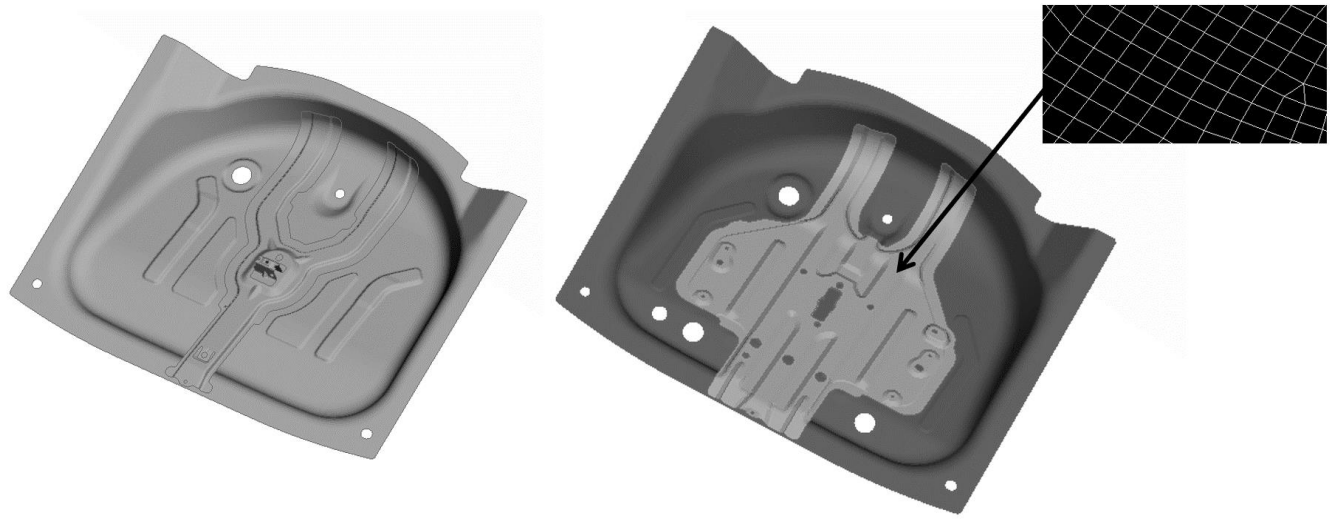

Figure 3.2. *(a) FE-model before visual inspection (b) FE-model after visual inspection of manufactured parts.*

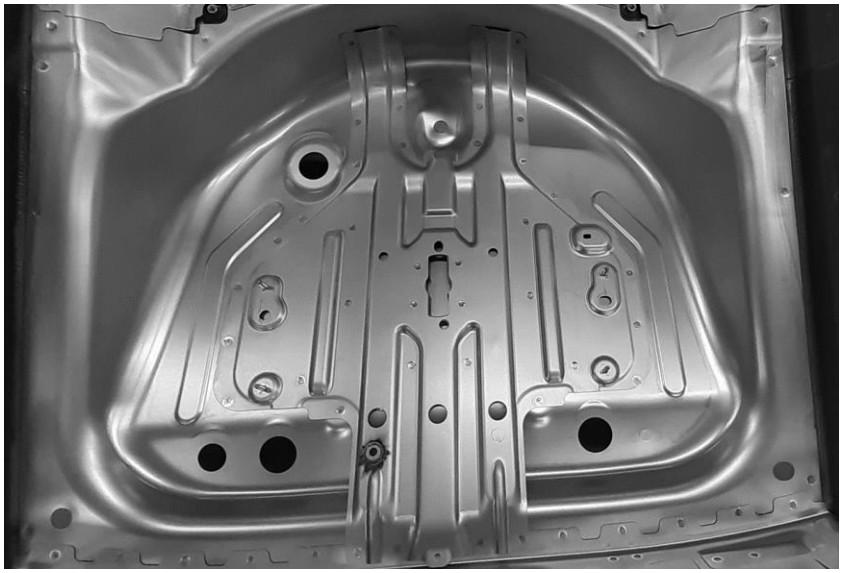

Figure 3.3. *Photo of manufactured floor panel rear.*

3.1.2 Element types

A mix of shell and volume elements were used in the model, with a nominal mesh size from previous mesh convergence studies at Volvo Car Corporation, as well as mesh quality criteria for NVH purposes. In Figure 3.4 an example of elements not fulfilling the quality criteria are seen in grey, compared to the black elements indicating that criteria are fulfilled.

For the shell mesh, linear isoperimetric quadrilateral elements (CQUAD4) and linear isoperimetric triangular elements (CTRIA3) elements are employed, with 6 degrees of freedom per node. The NASTRAN definition of these, references to the connected grid points and a shell property. The shell property of the element specifies for example the membrane thickness and material model. Where the thickness is not significantly smaller than other dimensions, solid elements are employed. Firstly, brick elements with six faces (CHEXA) and secondly wedge elements with five faces (CPENTA) are used.

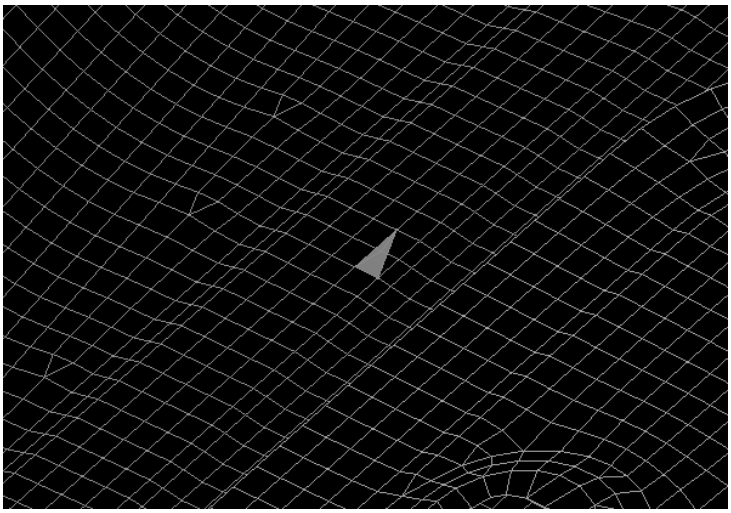

Figure 3.4. *Example of mesh quality criteria not fulfilled for initial mesh of introduced part.*

3.1.3 Connections

To connect different parts of the sub-assemblies, different connections are used. Bolts, adhesive lines, and spot welds are common. Using the connection manager in ANSA the connections can be adapted such that the FE-model represents the physical connection, for example regarding the size and location of a spot welds.

Connections can be modeled in different ways in MSC NASTRAN. In ANSA, a FE-representation with chosen parameters, material and other factors affecting the modelling are chosen and later realized. In this project the spot welds were modelled with RBE3 and HEXA elements, bolts are modelled with RBE2 and CBAR elements and adhesive lines with RBE3 and HEXA elements etcetera. For information about these element types see MSC Nastran User's Guide (HEXAGON, 2021, b) where these are explained in depth. For further reading on modelling of spot welds, the reader is advised to read *Modelling of spot welds for NVH simulations in view of refined panel meshes* (Eppler & Schatz, 2007).

3.2 Dynamic loading

During the pre-test planning several load cases were set up, where impacts and response locations were identified such that the modes could be observed. The loads were then applied using a dynamic loading condition in MSC NASTRAN. The loads were applied on the form:

$$P(f) = B(f)\, e^{i(\theta(f)+\theta-2\pi f\tau)} \tag{3.1}$$

Using this definition, a unit load with constant amplitude $B(f) = 1$, was applied over the frequency range, with chosen direction and excitation point, depending on which mode that should be observed. In Figure 3.5 two chosen load cases are presented, in (a) the load is applied at the upper left corner normal to the surface of the crossmember, and in (b) the load is applied on the side member in vertical direction in the plane. Using the first load case, modes with predominate z-movement can easily be observed under the condition that a nodal line is not existing in that particular mode. Further explanation of the pre-test analysis will be given later in the report.

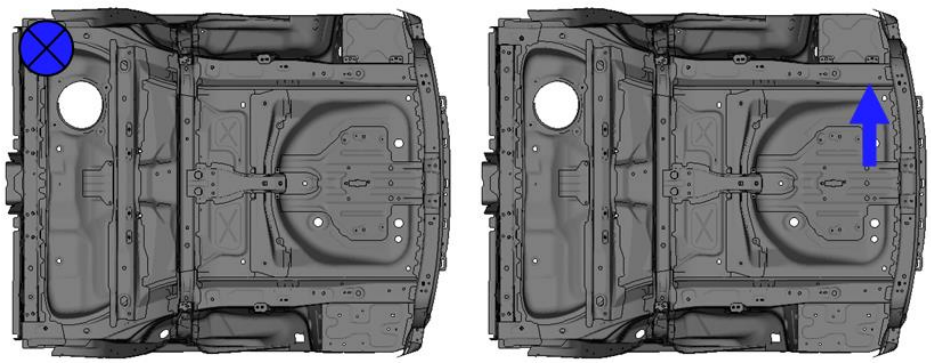

Figure 3.5. *Two of the decided load cases during pre-test analysis. (a) Excitation normal to the paper, (b) excitation vertical in the paper.*

3.3 Material data

The material data used for the sub-assemblies considered in this thesis work are linear isotropic materials, mainly defined by the Young's modulus (E), the mass density (ρ) and the Poisson's ratio (ν). The two main materials are steel and aluminum with the properties given in Table 3.1.

Table 3.1. *Main materials used in FE-model.*

Steel [linear isotropic]	
E	210 [GPa]
ρ	7850 [kg/m^3]
ν	0.3
Aluminum [linear isotropic]	
E	70 [GPa]
ρ	2700 [kg/m^3]
ν	0.3

In MSC NASTRAN the shear modulus is calculated from the above quantities from equation 3.2.

$$E = 2(1 + \nu) * G \tag{3.2}$$

3.4 Boundary conditions

Two set of boundary conditions were used for this project, one for each sub-assembly. Due to the differences in the two structures, the boundary conditions need to be adapted to what is feasible in the NVH laboratory. The floor is mounted on air bellows, a common construction for vibration isolation. These mimics the free-free conditions that can be used in simulation. Similarly, the side of the body is suspended in metal springs, also for mimicking free-free conditions, used in simulation. The equipment used in this project can be seen in Figure 3.6, (a) air bellow and in (b) metal springs.

In CAE two different approaches where considered, either modelling the physical boundaries such as the air bellows or using free-free conditions. Since the air bellows and springs will only be visible very low in frequency, less than the first flexible mode of the sub-assemblies, the latter option was considered in this thesis. In the measurement data the rigid body modes will thus be easily separated from the flexible modes. Avitabile (2001) argues that at least a 10:1 ratio between rigid body modes and flexible modes is necessary, but even at this level variation in frequency can be up to 5% in particular cases.

Furthermore, a second set of measurements were performed on the Floor Rear, altering the mounting of the air bellows. In Figure 3.7 the floor is placed upon the bellows directly, whilst in 3.8 the floor is placed in wooden blocks.

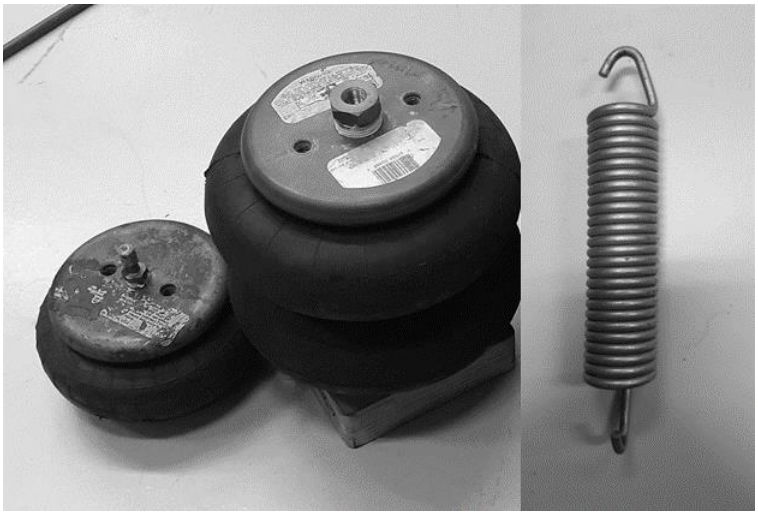

Figure 3.6. *Boundary conditions for testing, (a) air bellows for the body floor, (b) metal spring for suspending side of the body.*

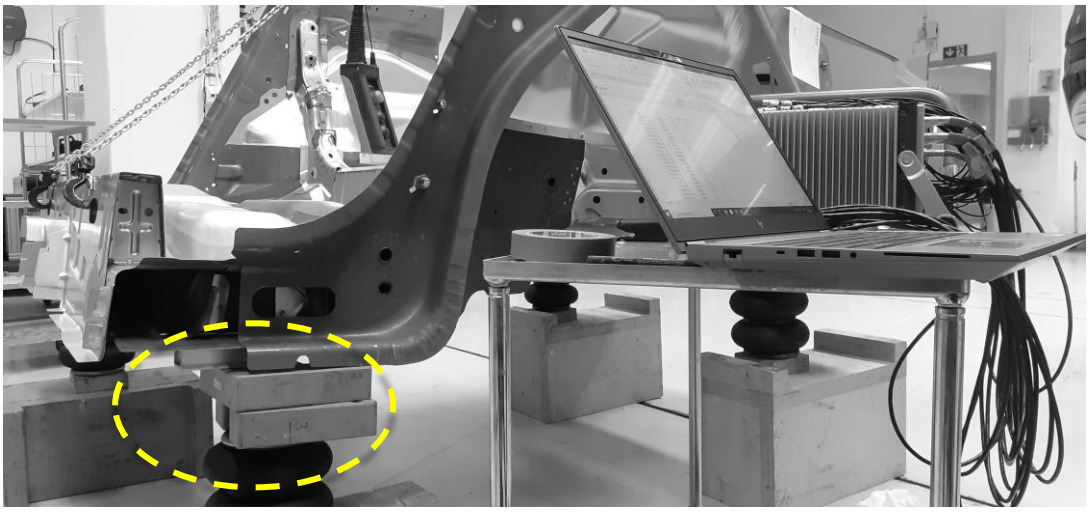

Figure 3.7. *Boundary conditions for test 1 on Floor Rear (BC1).*

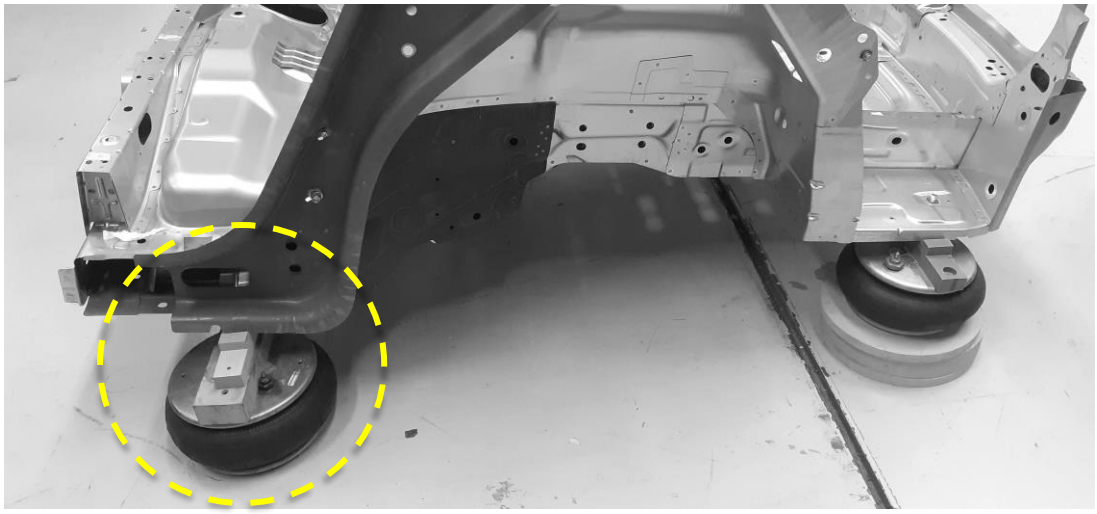

Figure 3.8. *Boundary conditions for test 2 on Floor Rear (BC2).*

3.5 Numerical simulations and pre-test planning

3.5.1 Normal modes analysis (NMA)

Setting up a NMA serves several purposes, two of which are to calculate the system's natural frequencies and mode shapes. The computation is an eigenvalue problem, solving the equation:

$$\boldsymbol{M}\ddot{\boldsymbol{x}} + \boldsymbol{K}\ddot{\boldsymbol{x}} = 0 \tag{3.3}$$

which is the equation of motion for an undamped free vibration. Furthermore, under the harmonic assumption, the solution to the eigenvalue problem reduces to solving the eigenequation recognized from basic courses in mathematics:

$$(\boldsymbol{K} - \omega^2 \boldsymbol{M})\,\boldsymbol{\Phi} = 0 \tag{3.4}$$

The analysis was set up as a script, specifying a chosen frequency range, for the two sub-assemblies in MSC NASTRAN. Results were visualized in post-processor META, whilst the eigenvalues could be obtained directly in the NASTRAN output files such as the f06.

3.5.2 Modal frequency response analysis (MFRA)

The results from the NMA are used in the MFRA in a subsequent step, where the mode shapes are used for uncoupling of the equation of motion. The procedure of uncoupling the equation of motion is described by for example Abrahamsson (2000), where physical quantities are transformed into modal quantities. The response is then calculated for the forcing function defined previously.

Two headers were developed, for NMA and MFRA in MSC NASTRAN. In these scripts the chosen FE-model was appended, and factors such as damping and dynamic loading could be adjusted more easily than using the pre-processor.

3.5.3 Pre-test planning

After computation of the mode shapes and natural frequencies, a pre-test planning was initialized. An engineering approach was used, studying the dynamical behavior of the structure, thus identifying sensor locations and excitation points capturing this. Simulations were employed (NMA and MFRA), together with studying the physical components since feasible assumptions must be made. In experimental modal analysis consideration must be taken regarding for example the excitation method. In this project an impact hammer was used, and thus a hammer must be able to physically reach the excitation point chosen in pre-test planning as in Figure 3.9. Thus, the optimal point from simulation perspective will in some cases not be the feasible in testing.

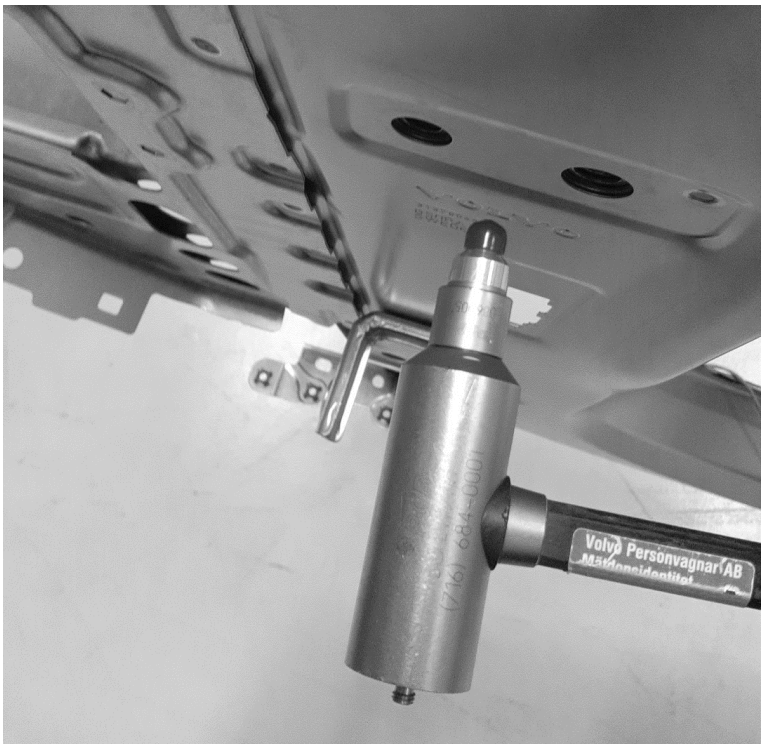

Figure 3.9. *Impact hammer with a tip, load cell and mass.*

The triaxial accelerometers should be able to identify all modes of interest, for example the Global Bending mode, Global Torsion mode and the Lateral Bending mode. Using META to visualize mode shapes, sensors can be placed at locations observing these. Furthermore, using frequency response analysis, excitation points can be studied to see if they excite a mode of interest or not, thus preparing the test so that when the laboratory is available, everything should be planned and known in advance. An important rule is to not excite nodal lines, which can be seen by the NMA or MFRA.

3.6 Testing and NVH-analysis

For performing the measurements two different systems were used in separate measurements, a PAK MKII and a LMS Testlab system. The ICS channels, where the triaxial accelerometers are inputted, are seen on the PAK hardware in Figure 3.10. Furthermore, in Figure 3.11 one test setup on the Floor Rear is seen, where thirteen accelerometers have been instrumented for a test using Simcenter LMS Testlab.

Figure 3.10. *PAK MKII system.*

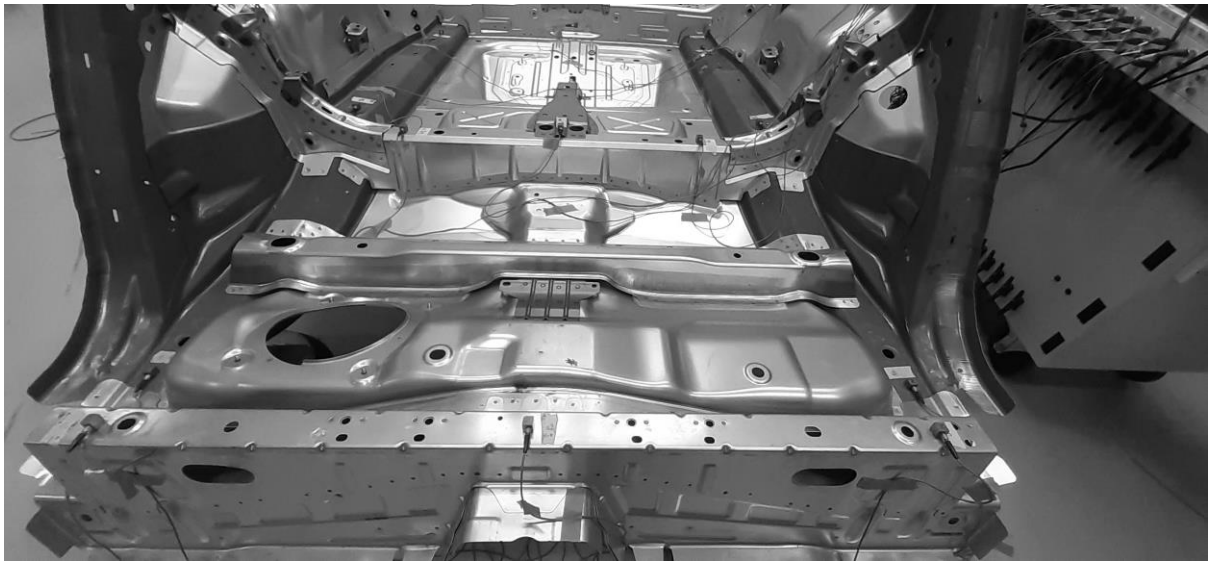

Figure 3.11. *Test setup on Floor Rear using Simcenter LMS Testlab.*

3.6.1 Calibration of measuring equipment

To be able to trust results from the accelerometers and impact hammer these should be calibrated before measurements. The resulting calibration factor from the calibration is then given as input to the software used when performing the measurements. A reference frequency of 159.2 Hz was used, together with a general guideline regarding the sensitivity. In this case that the measured accelerometer sensitivity must be within 5% more or less than a nominal value specified.

3.6.2 Performing tests and quality assessments

Once all the required input has been defined in PAK (Müller-BBM VibroAkustik Systeme GmbH, 2022), the measurement can be performed. It is then important that the sensors and impact locations have been named properly in the software. Then it is a matter of impacting and checking the quality of the measurements. A quality assessment tool that was used during measurements was the coherence function. It identifies how the output signal is related to the input signal, with the value one if two signals are completely related (Fu & He, 2001). Here also the input power spectrum is of importance since all modes of interest need to be excited, with a roll of above the frequency range of interest. It is of importance to have a flat input excitation forcing function, and a significant drop in the frequency range of interest should not be accepted. To be able to calculate the coherence an average of impacts must be performed, this number was set to 5 impacts. Furthermore, to obtain qualitative measurements, the settings were chosen in PAK to check for double hits or multiple impacts using the hammer. The same general procedure was used in Simcenter LMS Testlab, when performing the second set of measurements.

A suitable hammer tip is of importance when performing impact measurements. Several different tips were tested during this thesis, to be able to choose the tip with the best coherence function and input power spectrum. In Figure 3.12 it is seen that the chosen tip gives a good coherence in the lower frequencies where this project is conducted, whilst higher in frequency the quality is bad, and the data cannot be trusted.

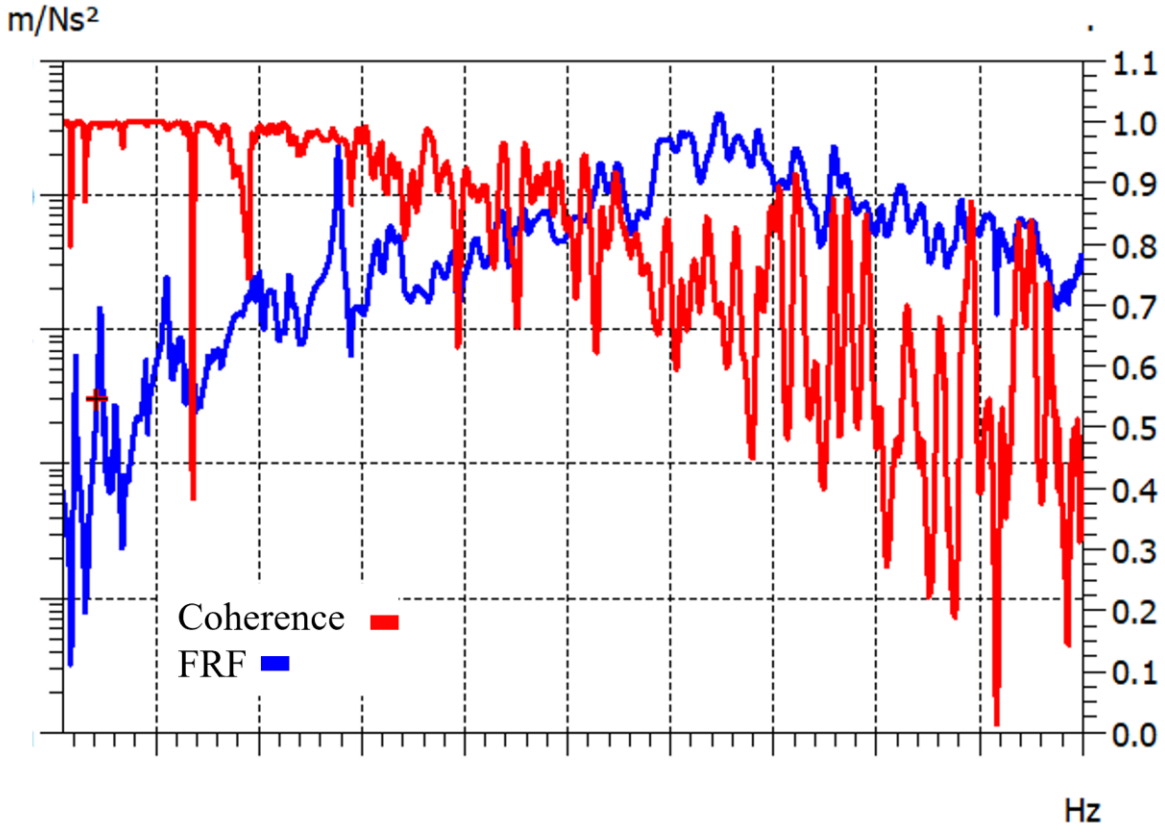

Figure 3.12. *Coherence and FRF from impact measurement in PAK.*

3.6.3 Identifying global modes directly from FRFs

For identifying global modes, the mode shapes are first studied using for example META with data from NMA. Using the mode shape of a torsion mode, seen for example from experimental modal analysis in Figure 3.14, the four corners can be identified by their phase. These points can then be studied in the context of the engineering and mathematical model presented earlier in this dissertation. Using real and imaginary parts, mode shapes can be identified solely from the frequency response functions if the load case and responses have been defined properly in simulation and in testing. For the torsion mode, the corners on the same diagonal should be in phase (sensor 1 and 13 in Figure 3.14), whilst the two diagonals should lie out of phase to each other.

In Figure 3.13 the torsion mode has been identified by using the imaginary and real part of the inertance. Here sensors 1, 3, 11 and 13 are placed on the outer corners of the Floor Rear (see Figure 3.14). Using this method, mode shape and resonance frequencies can be identified and compared between experiments and simulations for correlation purposes directly from FRFs without further processing of the data. In the figure below, the values have been hidden.

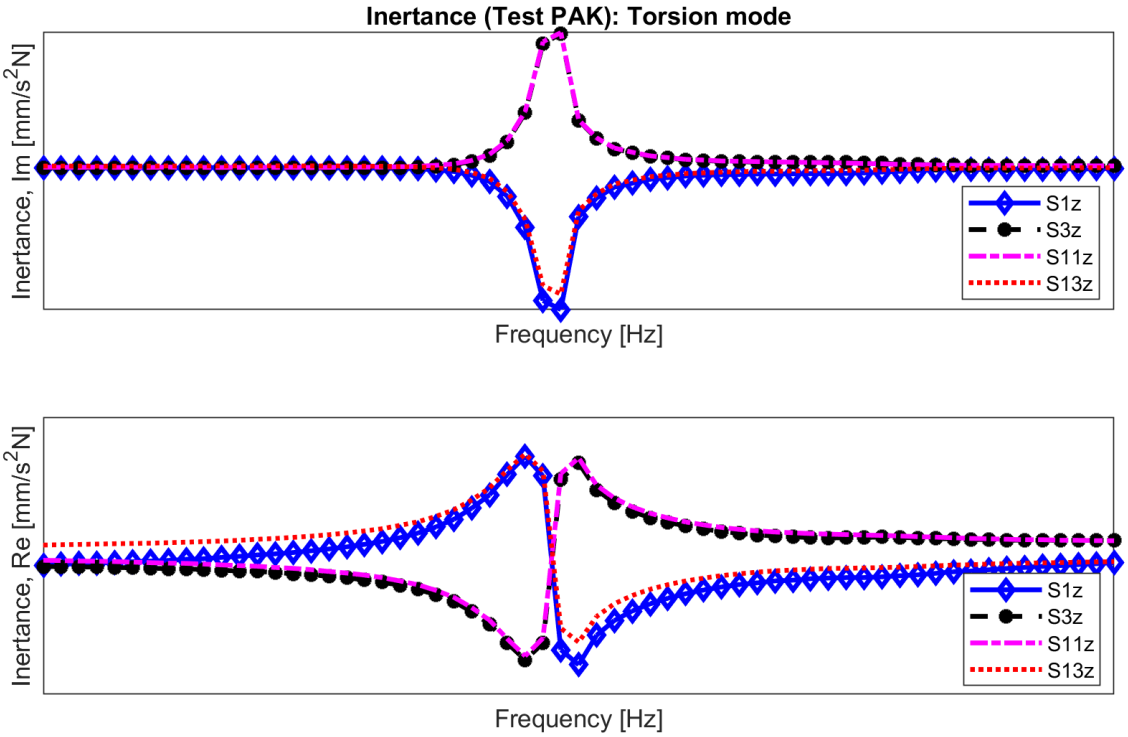

Figure 3.13. *Real and imaginary part of inertance FRF, obtained from PAK, load case (a).*

3.6.4 Experimental modal analysis using PAK and LMS Testlab

In addition to using FRF:s for estimating mode shapes, resonance frequencies and damping, experimental modal analysis can be used. In experiments not all degrees of freedom can be measured, in Figure 3.14 thirteen triaxial accelerometers have been used resulting in 39 degrees of freedom. The floor rear is then represented as line elements connecting the spheres, and the response can for example be visualized. In Figure 3.14 a torsion mode is seen, with a characteristic twisting motion of the Floor Rear captured momentarily in PAK.

In Simcenter LMS Testlab the PolyMAX method was used for experimental modal analysis. Similarly, as in PAK, a geometry (Figure 3.15) was defined using the locations of the sensors. After the geometry had been defined, together with other impact measurement settings, a roving hammer test was performed. The roving hammer test resulted in several frequency response functions available for curve fitting, which must be selected in the software as *Input Basket* items. Once the modal data selection is completed, a bandwidth is chosen for the analysis such that the modes of interest are represented during curve fitting. It is then of importance to not start or end the band, at a peak, but at a valley.

In the next step a stabilization diagram is automatically created in Testlab, as seen in Figure 3.16. There are five different symbols in the diagram with different meanings, such as new pole (*o*), stable frequency (*f)*, stable frequency and damping (*d)*, stable frequency and eigenvector (*v)*, and all criteria stable (*s)*. Here the poles can either be manually or automatically selected by the software. Repeatability is sought after when choosing which modes that represent the structure best. This means that columns need to be found where the specific modal solution has frequency and damping repeatable over the several steps in the stabilization diagram.

In the last step, the mode shapes can be visualized using the identified model. The resonance frequencies can then be compared to those from CAE, and mode shapes compared either visually or by using for example the modal assurance criterion. The damping can then be used to calibrate the model, by applying for example a modal damping as a function of frequency.

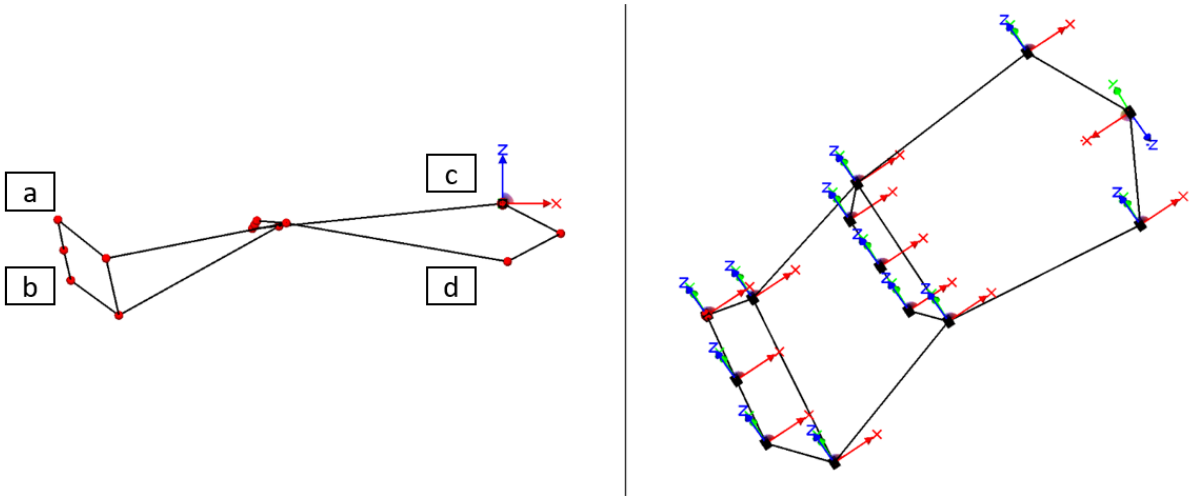

Figure 3.14. *Experimental modal analysis: Torsion mode generated from FRFs in PAK. (a) sensor 1, (b) sensor 3, (c) sensor 11, (d) sensor 13.*

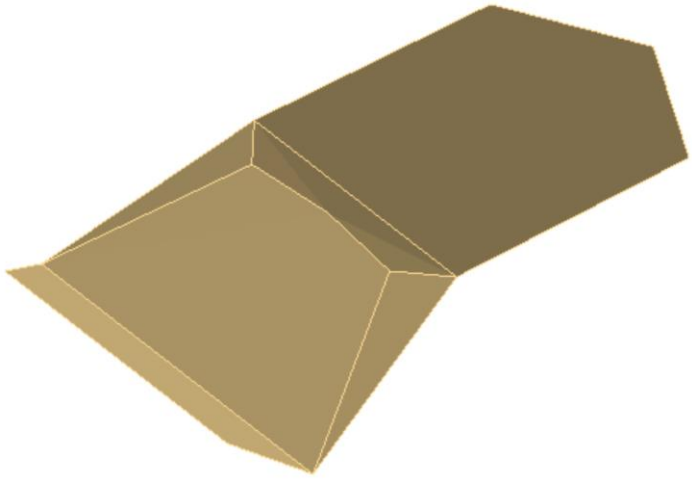

Figure 3.15. *Geometry representing Floor Rear in Simcenter LMS Testlab.*

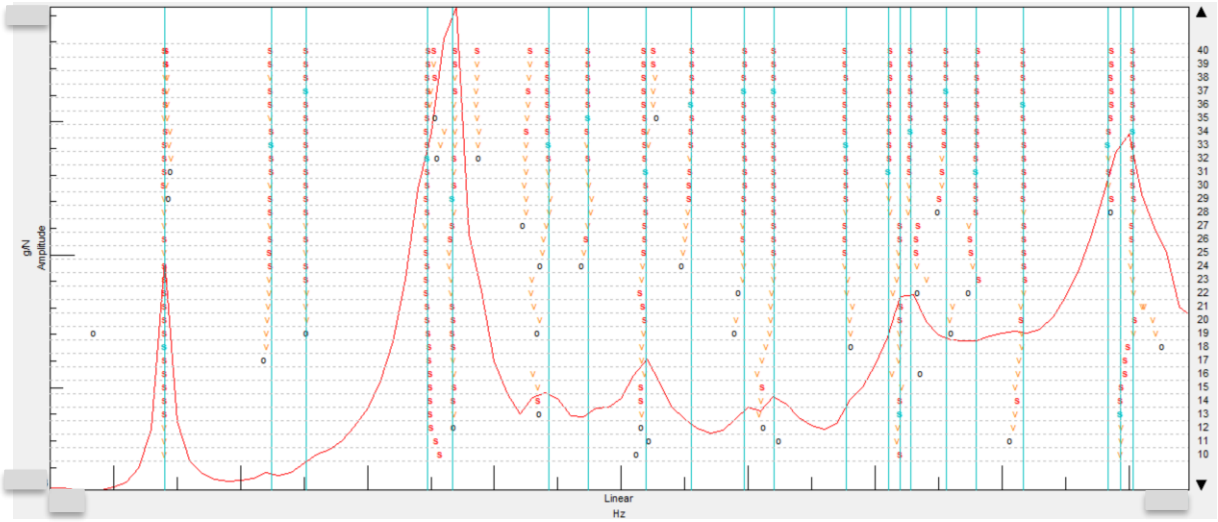

Figure 3.16. *Stabilization diagram in Simcenter Testlab for a certain set of FRFs. Automatically identified poles prior to manual selection.*

Once the modal parameters have been found using the curve fitting module in Testlab, further modules are available for analysis of the created model. First the *Modal Validation*, and secondly the *Modal Synthesis.* In the *Modal Validation* module, functions such as Auto -MAC are available for analyzing selection of modes in the stabilization diagram. When comparing a measurement against itself the MAC-numbers on the diagonal should be one, i.e., 100% similar modes. Furthermore, the off-diagonal terms should be closer to zero, otherwise the underlying modal model might be wrong. It can for example indicate that two similar modes have been selected.

As a further check of the curve fit, the *Modal Synthesis* module can be employed in Testlab. Here the synthesized FRFs are compared to the actual measured FRF, which can be used as a check that the model captures the overall dynamics of interest. Here it can be seen if an important mode was missed during the curve fitting process.

In Figure 3.17 the model from system identification is compared to the sum of measured FRFs to see if the curve fit is reasonably good. Testlab automatically calculates the correlation such that the two curves can be compared, in this case with 99% correlation, which shows that the no important modes should have been missed during curve fitting.

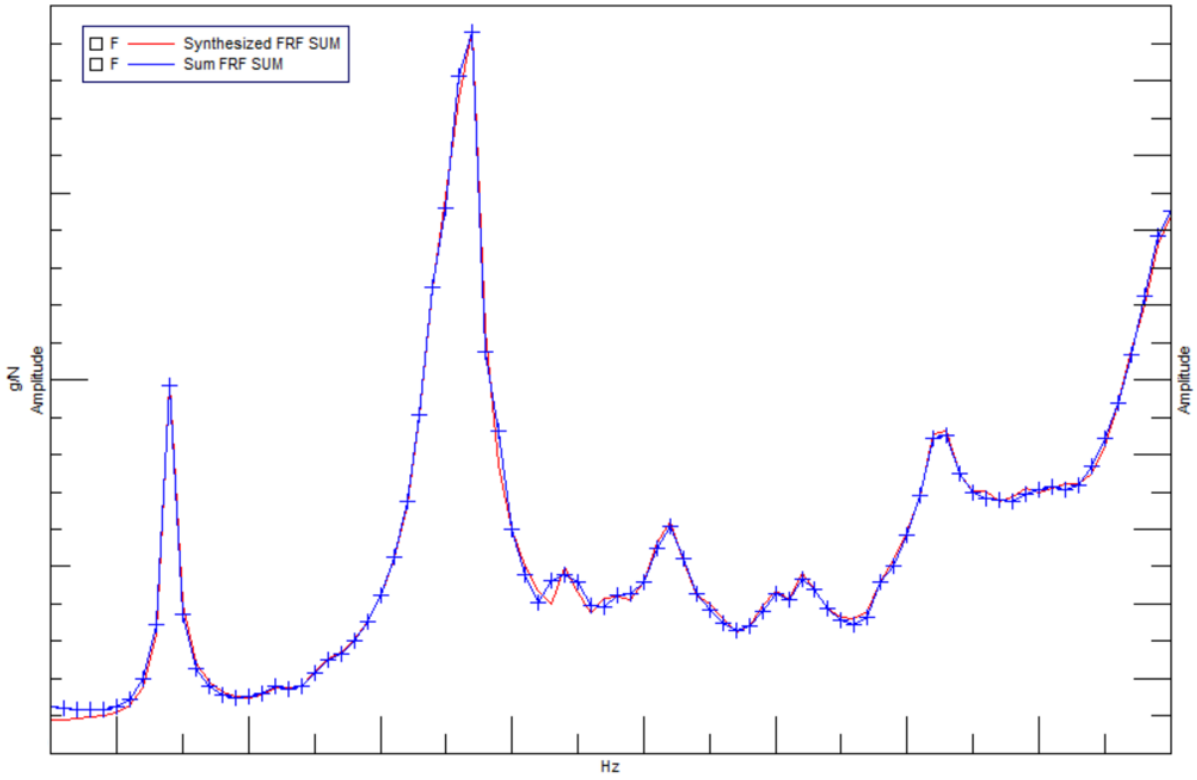

Figure 3.17. *Synthesized model compared to measured FRFs in Simcenter LMS Testlab, 99% correlation after curve fit. Sum of FRFs.*

3.7 Correlation procedure

Once experimental and numerical results have been gathered the correlation procedure is the subsequent step. An overall scheme is given in Figure 3.18, to show the iterative process. Using simulation and experimental results different criteria are studied, for example difference of natural frequencies and similarity of mode shapes using for example MAC. If the criteria are fulfilled the model is sufficiently good for its intended purposes. Otherwise, the model might need modifications, and new simulation results need to be obtained for further checks against the experimental input. During an iterative process, uncertainties can be identified and analyzed.

In the methodology above several different techniques have been described on how to correlate test and simulation data. One example is if to use an identified model as in EMA, or if to use a more direct approach using FRFs without system identification. These can then either be used separately, or they can assist each other depending on the situation.

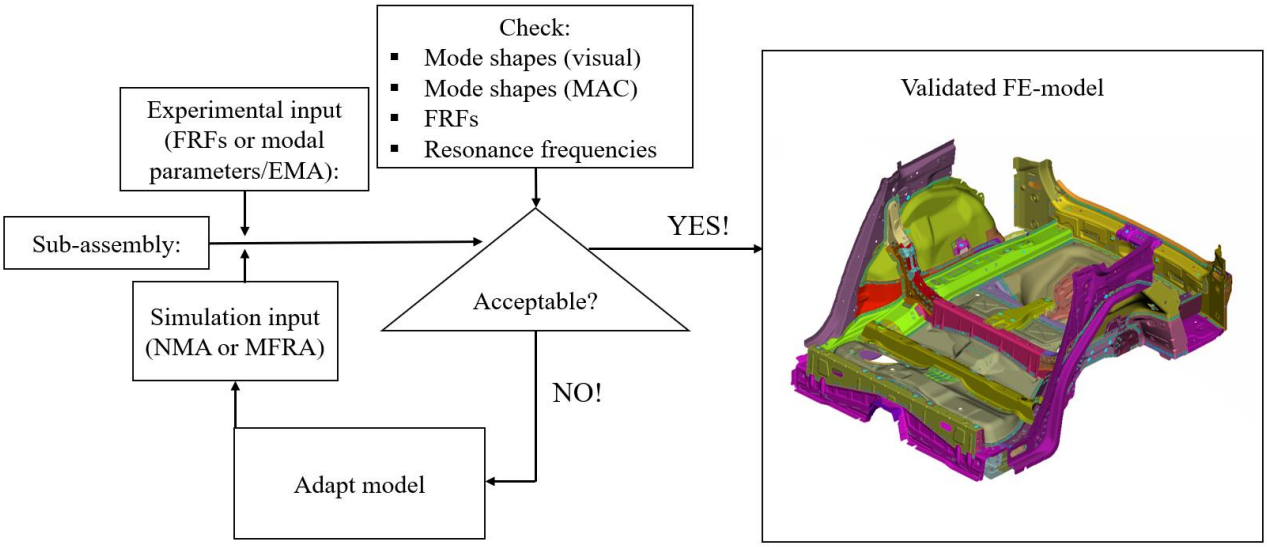

Figure 3.18. *Correlation procedure using simulations and experimental data.*

4. Results and Discussion

During correlation an engineering approach was used, studying physical explanations why results may differ and how the results are sensitive regarding the different modelling uncertainties. Special consideration has been taken to certain areas of the modelling, for example adhesives, weld spots, varying thickness, and the resulting mass. Correlating these differences once at a time for each sub-assembly uncertainties are localized and clarified.

Results will be presented for the Floor Rear and lastly, a comparison to the Body Side Outer will be made. The results will either be shown without values on the axis, or with normalized values in some cases. The reason for this is that resonance frequencies can be sensitive information for automotive companies like VCC. However, the same conclusions can be drawn using this data.

4.1 Pre-test and modal analysis

4.1.1 Nodal lines and excitation

The nodal lines can be approximated using META, seen in Figure 4.1 as green areas. For each mode these can be studied to see where the structure doesn't move, i.e., zero displacement. Using this information, it is known were not to excite a structure to be able to observe that mode from a certain FRF. In Figure 4.1, *a*, *b*, and *c* shows examples of points not to excite if these three different modes are to be observed after an impact in vibration testing.

To excite the Global Torsion mode two simulations were submitted. In Figure 4.2 two drive point responses are plotted to show the difference between these load cases. For the red line, load case *a* from Figure 3.5 has been used. For the blue line, sensor 1 seen in Figure 3.14 has been excited in *z*-direction (normal to the vehicle floor).

As can be seen in Figure 4.2 the Global Torsion mode is not captured in a good way by exciting on the approximate nodal line, and thus exciting on this point would have been useless for correlating the torsion mode. For load case *a*, a clear peak is visible indicated by the asterisk. Both curves show data from a modal frequency response analysis using NASTRAN.

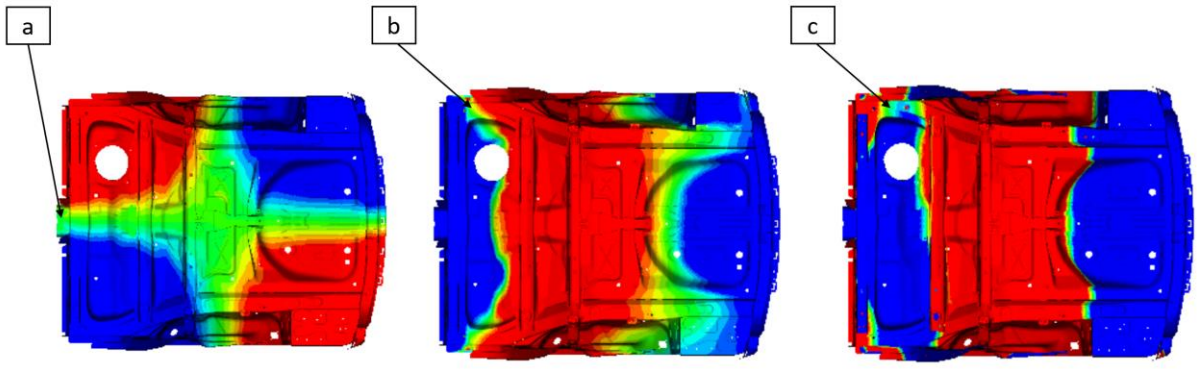

Figure 4.1. *Approximate nodal lines in green, for Global Torsion (left), Global bending (middle) and Lateral Bending (right).*

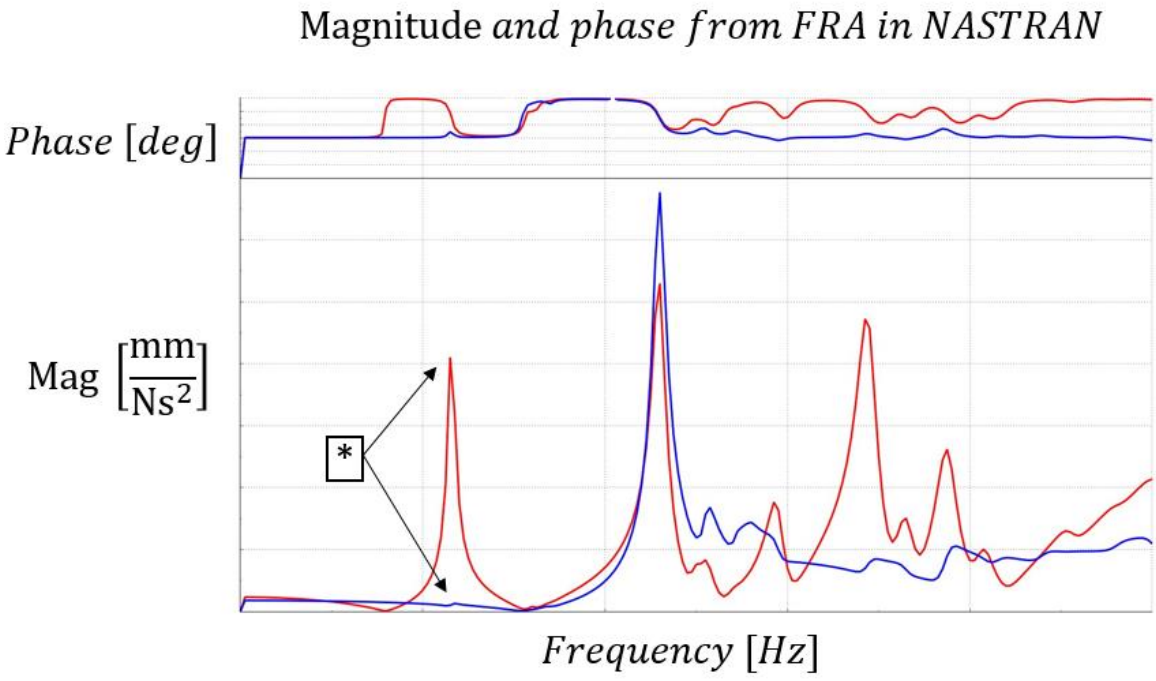

Figure 4.2. *Drive point responses with clear peak for chosen load case (red curve), and unclear peak for inappropriate load case (blue curve) at the asterisk.*

4.1.2 Global modes (NMA & EMA)

Using MSC NASTRAN for normal modes analysis and Simcenter LMS Testlab for experimental modal analysis, the modes shapes of the studied structures were obtained. During correlation three main modes were studied when comparing mode shapes and resonance frequencies. These were a global torsion mode, a global bending mode and a lateral bending mode all of which are identified in Figure 4.3 below from testing and CAE. Thirteen sensors were chosen such that these modes could be observed during testing, as shown in Figure 4.3. On the two first modes the z-displacement is dominating, and on the last mode the y-displacement is dominating.

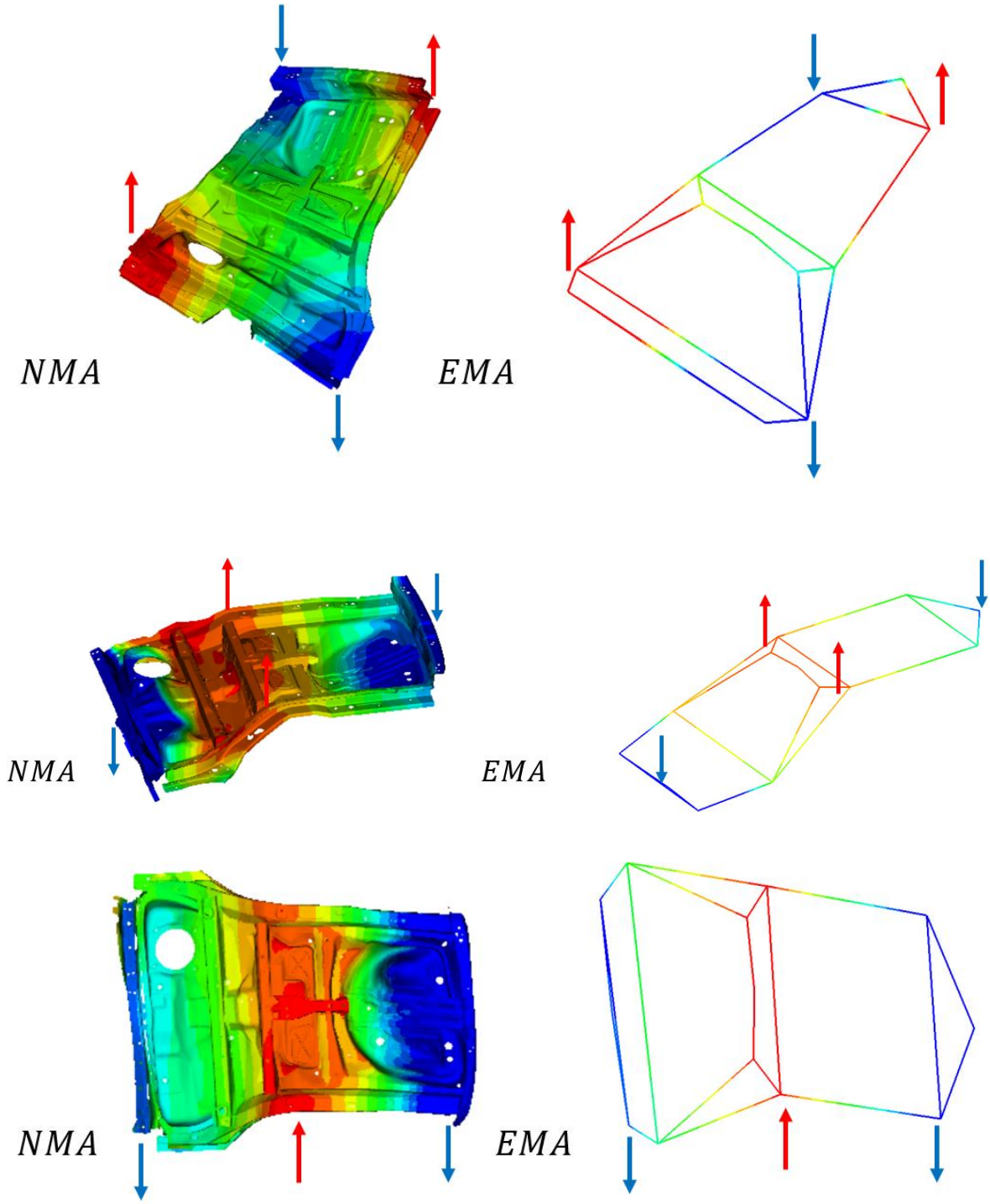

Figure 4.3. *Global modes used for correlation, from simulation and testing on Floor Rear. Captured momentarily in META and later in Simcenter LMS Testlab after curve fit of FRFs.*

4.2 Effect of boundary conditions

As mentioned in section 3.4, two different sets of boundary conditions (BCs) were used during measurements. In this way the effect on the dynamical properties due to the boundaries can be studied in some more detail, to further understand the results during correlation. As can be seen when comparing the two sets, the second set of BCs imposes extra constraints since, the wooden block restricts some movement creating a moment. This effect can be studied using for example EMA using FRFs from measurement one and two. The global modes are then of special interest, and thus the Global torsion, Global Bending and Lateral bending modes are studied.

In Table 4.1 frequencies of the global modes are compared, with increasing frequency to the right. As can be seen the second set of boundary conditions presented in the method, are adding constraints. The presented table shows the importance of properly mimicking free-free conditions when comparing to simulation and shows some of the uncertainties in the test results as well. Avitabile (2001) has shown in his articles that a ratio larger than 10:1 between rigid body modes and flexible modes in a test setup, can still give a 5% variation in frequency on the first flexible mode. Like the results presented in this dissertation, Avitabile (2001) shows that also the second flexible mode can be affected. During correlation, the first set of boundary conditions (BC1) were used since they more properly mimic the conditions in simulation, with an acceptable ratio between flexible and rigid body modes.

Table 41. *Global modes identified from EMA using FRFs from measurement 1 and measurement 2.*

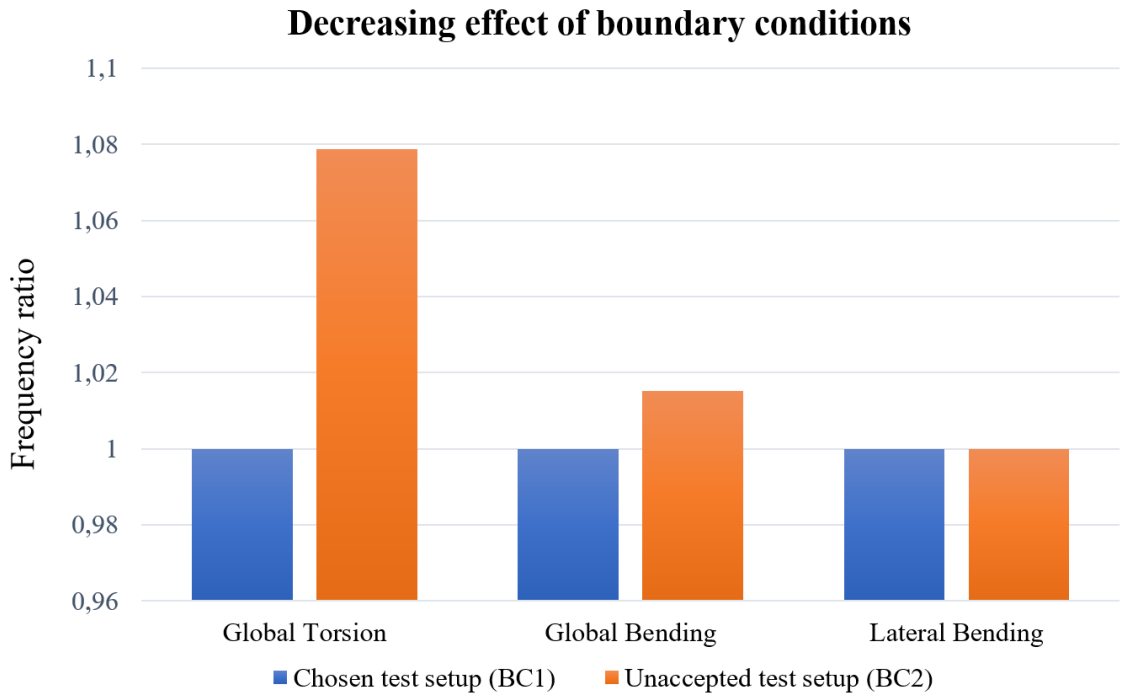

4.3 Correlation of mass

The natural frequency of a structure is related to the mass and the stiffness, which can in some cases be simplified to $\omega_0 = \sqrt{\frac{k}{m}}$. It is thus seen that a structure's mass and stiffness is important for correlating for NVH-purposes. Thus, a first step is to see that the mass of the FE-model is acceptably close to the physical parts. To correlate the mass the physical parts were weighted two times using separate measuring equipment in the NVH-laboratory, which resulted in mass M_t. Using NASTRAN output files, the FE-models mass M_n, was obtained and these two values could be compared.

A small difference was observed, most likely caused by the thickness being modelled as uniform when stamping simulation results are not introduced in the FE-model. When introducing the mapped thickness, the mass of these parts was closer to the measured weight. Thus, introducing a mapped thickness would increase the accuracy of the mass.

To see if the results are sensitive against the difference between FE-model and physical parts, a drive point measurement was studied over a frequency range, as seen in Figure 4.4. Here the density has been changed such that the FE-model has the exact same weight as the physical part and this plot is compared to the original density. It can be noted, the difference in mass results in no change in frequency on for example the first flexible mode, i.e., the Global Torsion mode.

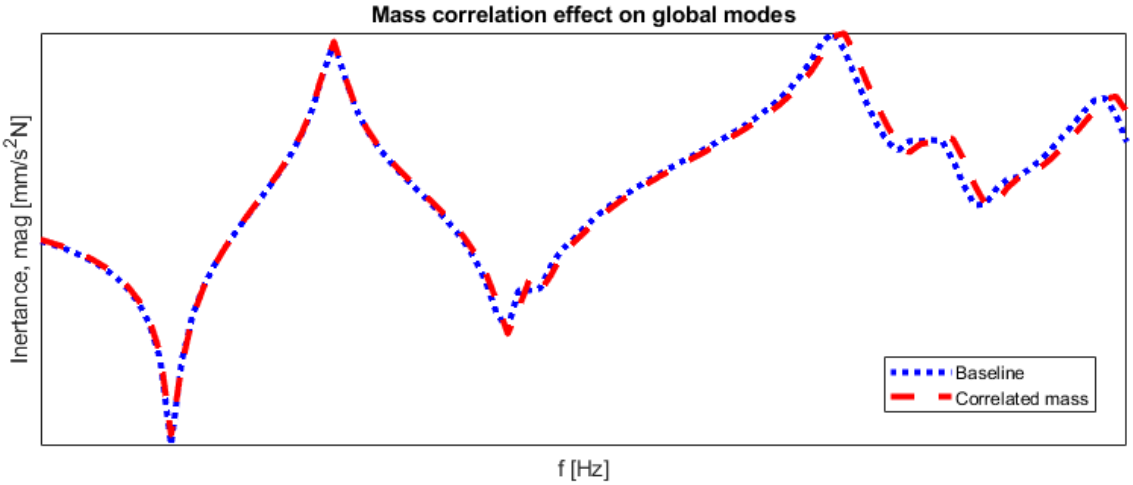

Figure 4.4. *Drive point FRF, studying effect of mass difference between measured weight and model weight. Load case (a), response in sensor* 1 *in z-direction.*

4.4 Correlation of connections

A common cause of uncertainties in FE-modelling is the connections. Also, during manufacturing uncertainties always exist regarding size and location of spot welds. Furthermore, two similar components produced will not be identical. For example, the size of spot welds follows a normal distribution and is not exact. In this report the welds and the adhesives have been studied, regarding sensitivity and correlation.

4.4.1 Adhesive

The material data used for the FE-model is assumed for a final car, in other words when the car rolls of the end of the production line, and thus reflect how it will behave when used by a customer. In this thesis sub-assembly correlation is evaluated and thus the various assemblies were obtained from an earlier step in the factory, and thus some changes are to be expected. In Figure 4.5 an adhesive is seen on one of the parts, clearly not stiff from curing processes.

Thus, the material data cards were adjusted to a more correct value. Since the adhesive is less stiff the eigenfrequencies will instinctively drop when adjusting the model in this way. In Figure 4.8 a drive point FRF has been employed, to highlight some different FE-model versions in this project. First the unadjusted model is seen, followed by adjusted adhesives and connections. As expected, the *Adhesives* plot has translated to the left, since the model should be less stiff before curing. This points out some of the steps necessary when correlating assemblies of the body, and also shows the effect of the adhesive before and after curing.

4.4.2 Welds

As previously mentioned, the size and location of spot welds can be adjusted in ANSA, which was the next step of the correlation procedure. Similarly, as the adhesives, spot welds provide stiffness to the structure. Some weld nuggets are seen in Figure 4.6 and in Figure 4.7, where an unconnected flange has not yet been welded together. The results from correlating the welding can be seen in Figure 4.8, where the FE-model has been adapted to follow the current step of the assembling process.

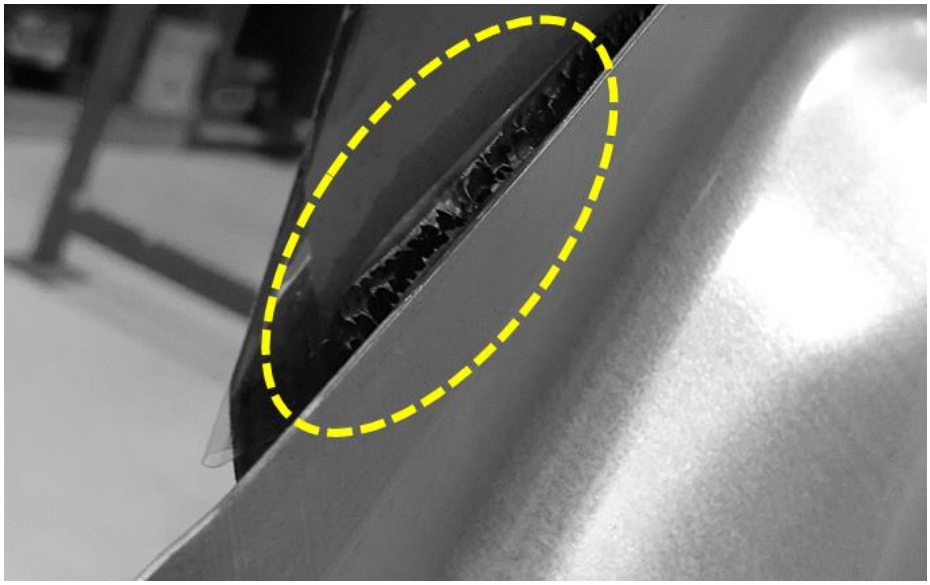

Figure 4.5. *Adhesive, before curing the BIW.*

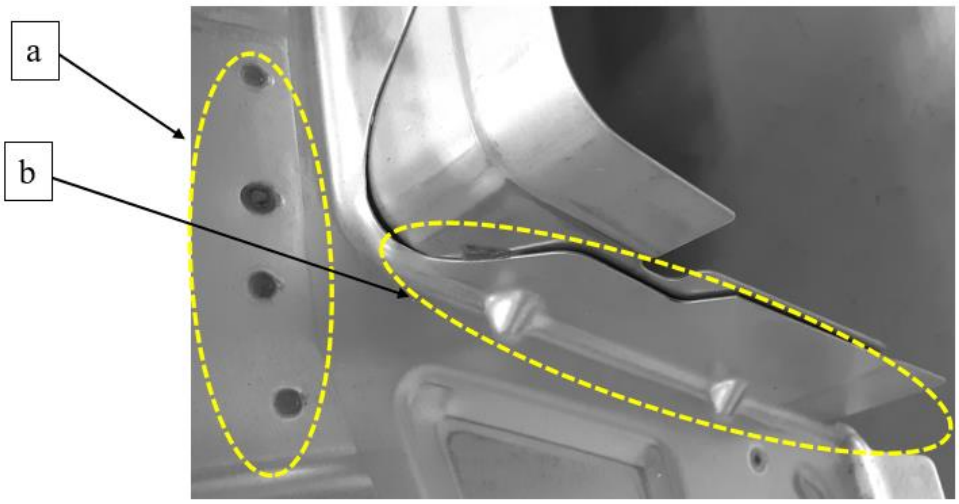

Figure 4.6. *(a) Four weld nuggets, (b) unconnected flange due to assembling process.*

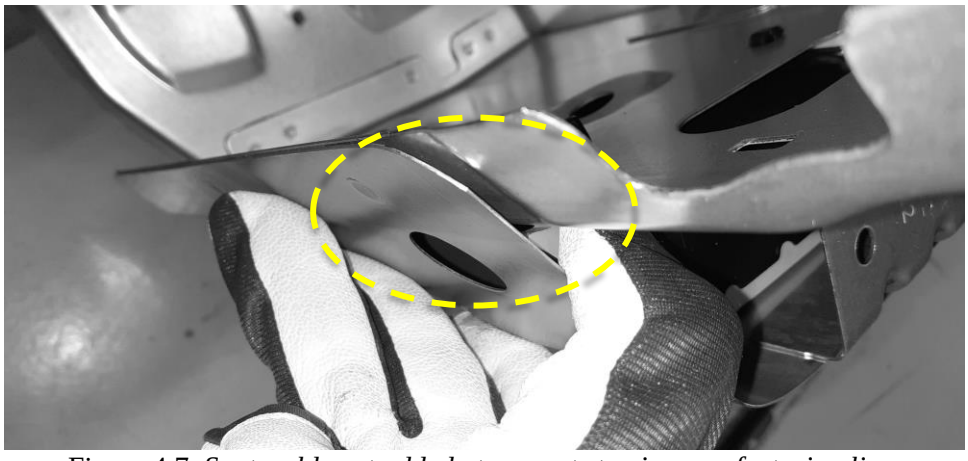

Figure 4.7. *Spot welds not added at current step in manufacturing line.*

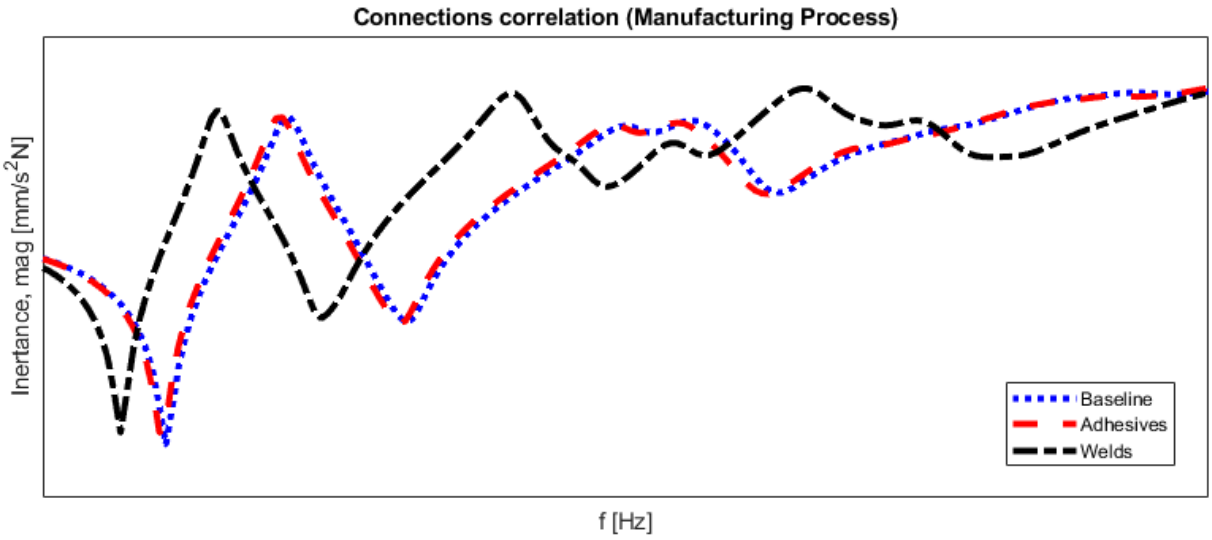

Figure 4.8. *Drive point response, studying effect of adhesives and welds. Load case (a), response in sensor* 1 *in z-direction.*

Table 4.2. *Effect of connections on first flexible eigenfrequency in frequency range studied.*

FE-version	Normalized eigenfrequency [Hz] Min-Max scaling	Percentage [%] of baseline models eigenfrequency
Unadjusted model	1	100
Adhesives	0.87	97.59
Welds	0	81.03

As can be seen the welding has a larger impact on the results than the adhesives for this specific case, suggesting that the results are more sensitive to the weld parameters. The first frequency in the frequency range is also studied in Table 4.2. The baseline model cannot be used when correlating sub-assemblies since the modelling of connections are not adjusted for this purpose. The difference in percentage on the resonance frequencies is as high as 20% which means that this cannot be overseen. Whereas the Young's modulus of the adhesive affects the stiffness of the overall structure, translating the curves to the left, the welds also affect the complete dynamical behavior introducing new peaks in the studied frequency range.

4.5 Damping study

The effect of is clearly seen in Figure 4.9, with an effect on the magnitude of the peaks between the two simulations. The blue curve has a measured damping from a BIW, whilst the red curve shows the FRF after the damping has been measured for the specific sub-assembly. Thus, it can be understood that the damping of the system is of high importance during CAE-work, for trusting the simulation results the damping must be correlated.

Damping is one factor that cannot be decided from simulations only and experimental data is crucial. In the FE-model a loss factor had previously been defined in the model from another measurement at VCC for a complete BIW. However, for the correlation work in this dissertation new damping values were decided for correlating parts of the body. In the methodology two different methods of deciding the damping were shown, a direct method using e.g., PAK (Müller-BBM VibroAkustik Systeme GmbH, 2022) or by curve fitting using Simcenter LMS Testlab (Siemens, 2022). The damping obtained from Testlab showed similar results and are thus not considered further.

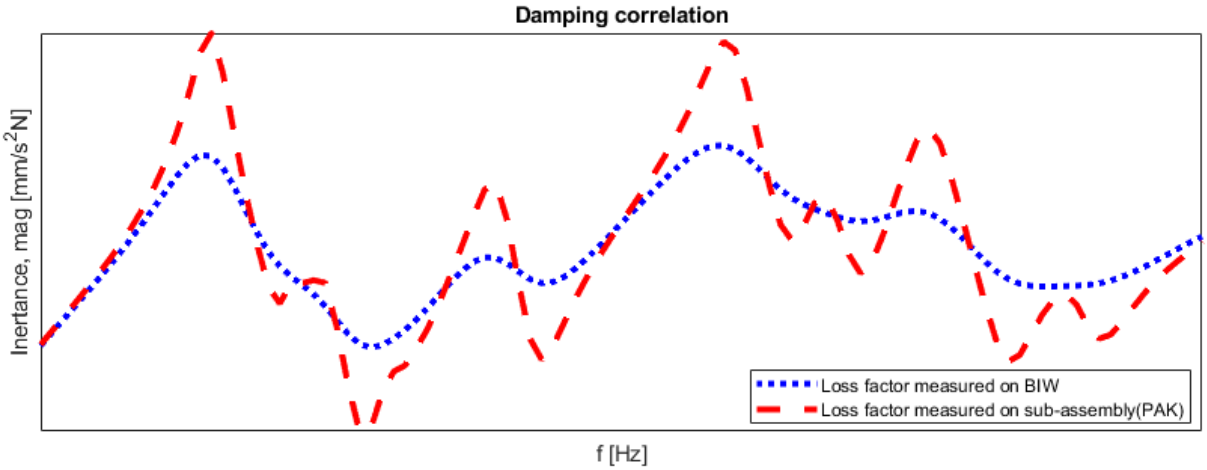

Figure 4.9. *Effect of measured damping on magnitudes of FRFs.*

Table 4.3. *Sensitivity of damping on three studied peaks.*

	Percentage [%] of unadjusted models' peak magnitude
Peak 1	242
Peak 2	171
Peak 3	213

To see more clearly the effect of adjusting the damping in NASTRAN, the percentage of the unadjusted models' damping can be read in Table 4.3 for the three of the main peaks. The peak magnitude is at about 242 % of the unadjusted magnitude at the first peak, which indicates that correlating the damping is of high importance when studying for example dynamic stiffness if results are to be trustworthy.

4.6 Mapped thickness

The last physical uncertainty studied during correlation in this dissertation, is the thickness distribution. Often the thickness is modelled as being uniform which gives uncertainties in both stiffness and mass, which can be reduced by implementing results from forming simulations. The effect of introducing mapped thicknesses has already been discussed during the correlation of the mass, where it was seen that introducing the mapped thickness increased the accuracy. The sensitivity can also be discussed, to see if the assumption of a uniform thickness is reasonable or not.

In Figure 4.10, the drive point response is studied for a simulation using uniform thickness (blue curve), and with mapped thickness in the side-members of the Floor Rear (red curve). As can be seen the resulting eigenfrequencies are somewhat translated to the left, indicating that the side-members are less stiff than modelled with uniform thickness. This uncertainty has a larger impact than for example the mass, where the first eigenfrequency in the interval did not change.

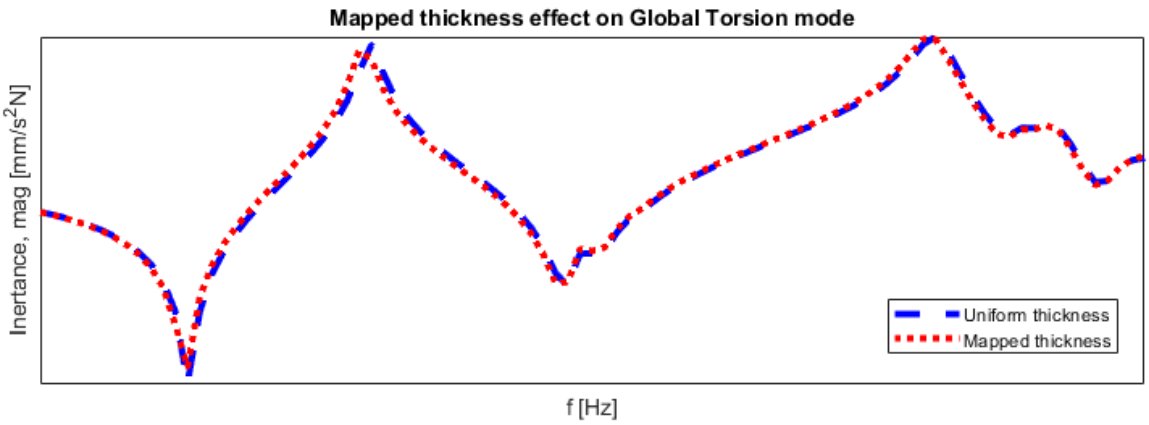

Figure 4.10. *Effect of mapped thickness on side-members of Floor Rear.*

Table 4.4. *Effect of mapped thickness on resonance frequency.*

FE-version	First resonance frequency in studied frequency range [%] of uniform thickness
Uniform thickness	100
Mapped thickness (side members)	98
Mapped thickness (side members/lower C-pillar/crossmembers)	98

In Figure 4.10 the side-members were modelled using mapped thicknesses from LS-DYNA (ANSYS, 2022) metal forming simulations. Since introducing a thickness distribution affected the results, further parts were introduced as well to study the sensitivity. Such as the lower inner C-pillar and the crossmember rear. In Table 4.4, the results of these changes are presented.

As can be seen in the table, a 2% drop is seen when mapping the thickness on the side members. The difference by introducing further parts could only be seen when studying decimals. This can be explained by looking at Figure 4.11, where the strain energy density is plotted on the Floor Rear. Darker colors are representing a higher strain energy density. As can be noted, for the studied mode, the strain energy density is higher at the side members than in the rest of the structure. Thus, the 2% drop can be explained, followed by less contribution by other parts at this specific mode.

The effect of introducing mapped thicknesses can thus be discussed. The effect on the correlation is limited and there may also be other production related effects to consider, nominally identical components have different dynamical properties as shown by Dorendorf (2017). This, however, cannot be said for the correlation of connections where large percentual differences were observed.

Figure 4.11. *Strain energy density on studied mode, from NMA.*

4.7 Comparison to test data

In this section the comparison to test data will be the focus, which follows the procedure described in the theory and method regarding identification of global modes using real and imaginary parts of a transfer function. This method is identifying certain important modes, so that that during correlation and identification of uncertainties, the same physical modes are being compared and the effect on these can be studied in detail.

This way each eigenfrequency is directly identified also in terms of the mode shape and not only a mode number. To compare mode shapes between testing and CAE, the modal assurance criterion (MAC) will be used as a final check to assure that the correct global modes have been identified. Only one iteration is shown below, since adding more iterations does not give any extra insight to the dissertation. However, the identification presented was used in a loop during this project.

4.7.1 Global modes & eigenfrequencies

The resulting differences between test and simulation eigenfrequencies are compared in Table 4.5. Here the global torsion, global bending and a lateral bending mode are compared regarding resonance frequency and similarity of mode shapes i.e., MAC numbers. As seen the difference between test and simulation eigenfrequency is around 3% or below, and similarly, the MAC numbers are above the acceptable level of 95% for these specific modes.

Table 4.5. *Overall comparison between CAE and test data. Floor Rear*

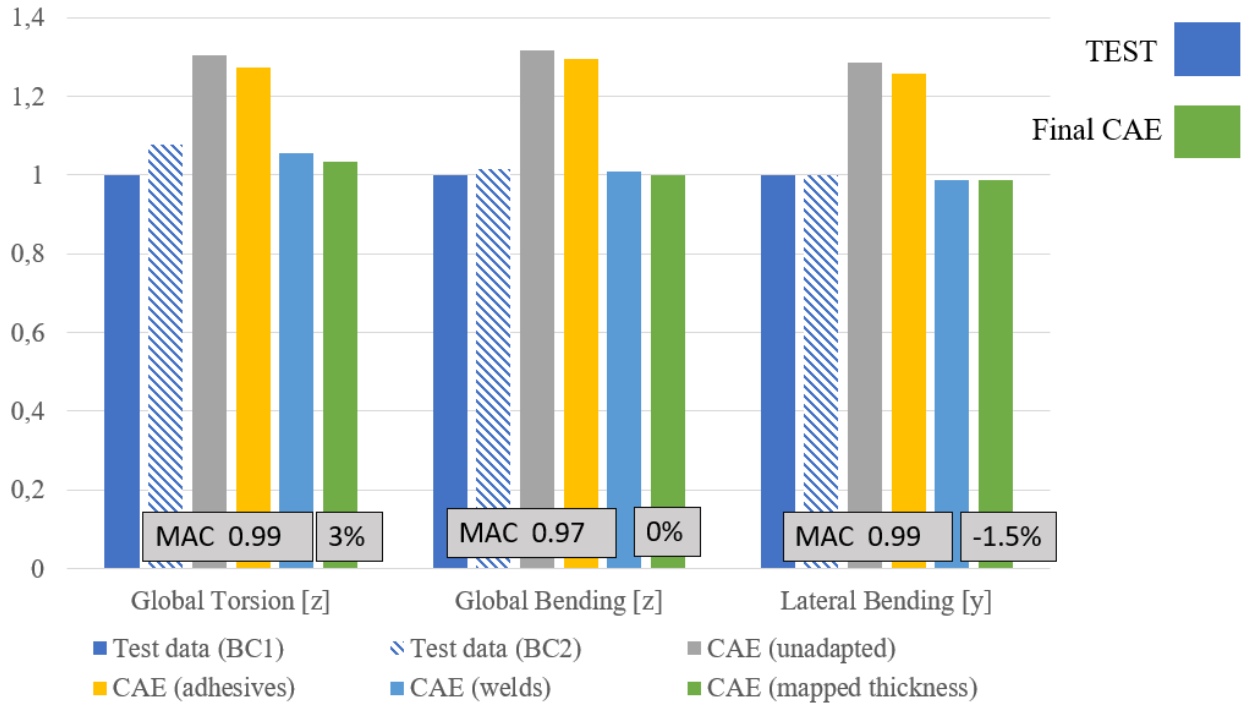

The identification of these main modes has followed the direct method presented in the methodology of this thesis. Two main load cases have been set up during pre-test planning for these modes, one exciting in *z* and one exciting in *y* (Figure 3.5, *a*, and *b*). The response has been taken at 13 accelerometers, numbered 1 to 13 (Figure 3.14). Since the accelerometers are triaxial the response direction is also given in the plots presented below.

In Figure 4.12 the Global torsion mode has been identified on the Floor Rear, using measurement data (to the right) and simulation data (to the left). In Figure 4.13 one way of identifying the Global Bending mode is shown, and in Figure 4.14 the Lateral Bending mode has been identified directly from FRFs. By identifying where the real part cuts the x-axis the resonance frequencies can be compared.

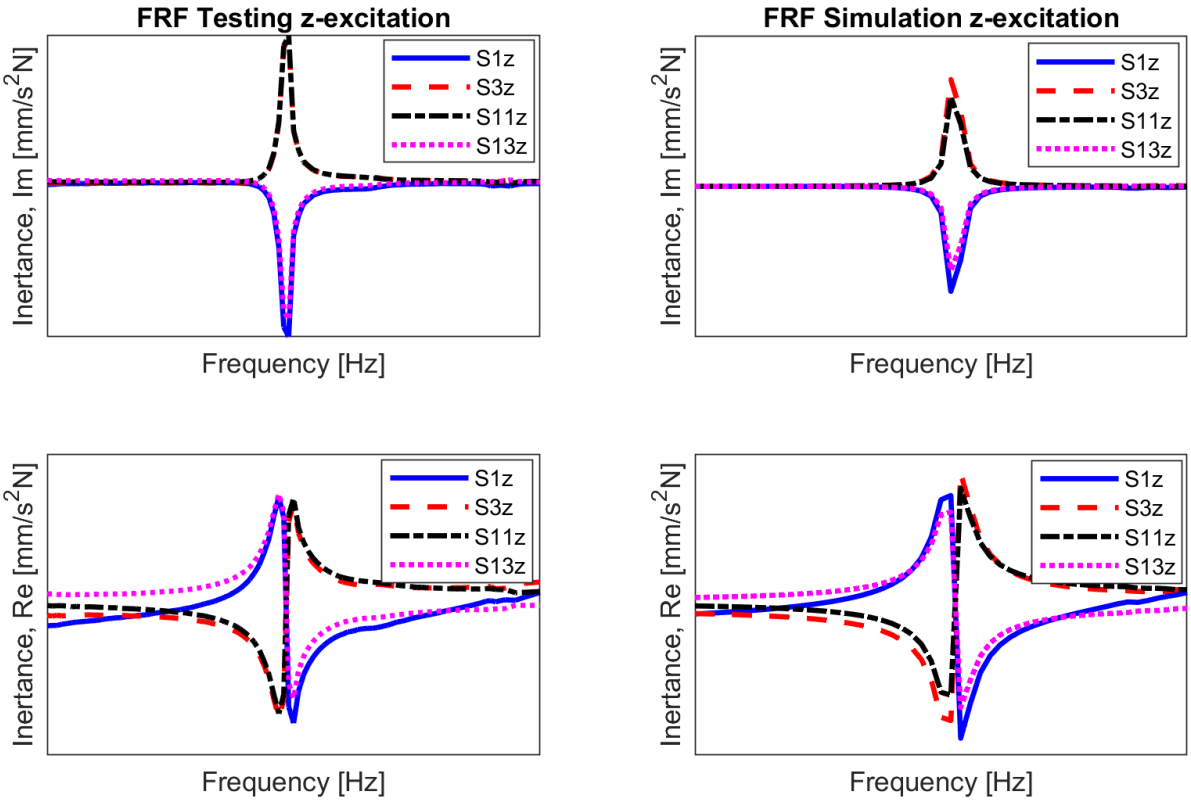

Figure 4.12. *Test (left) and simulation (right) results, real and imaginary part of inertance using z-response at four sensors. Global torsion identified from FRFs.*

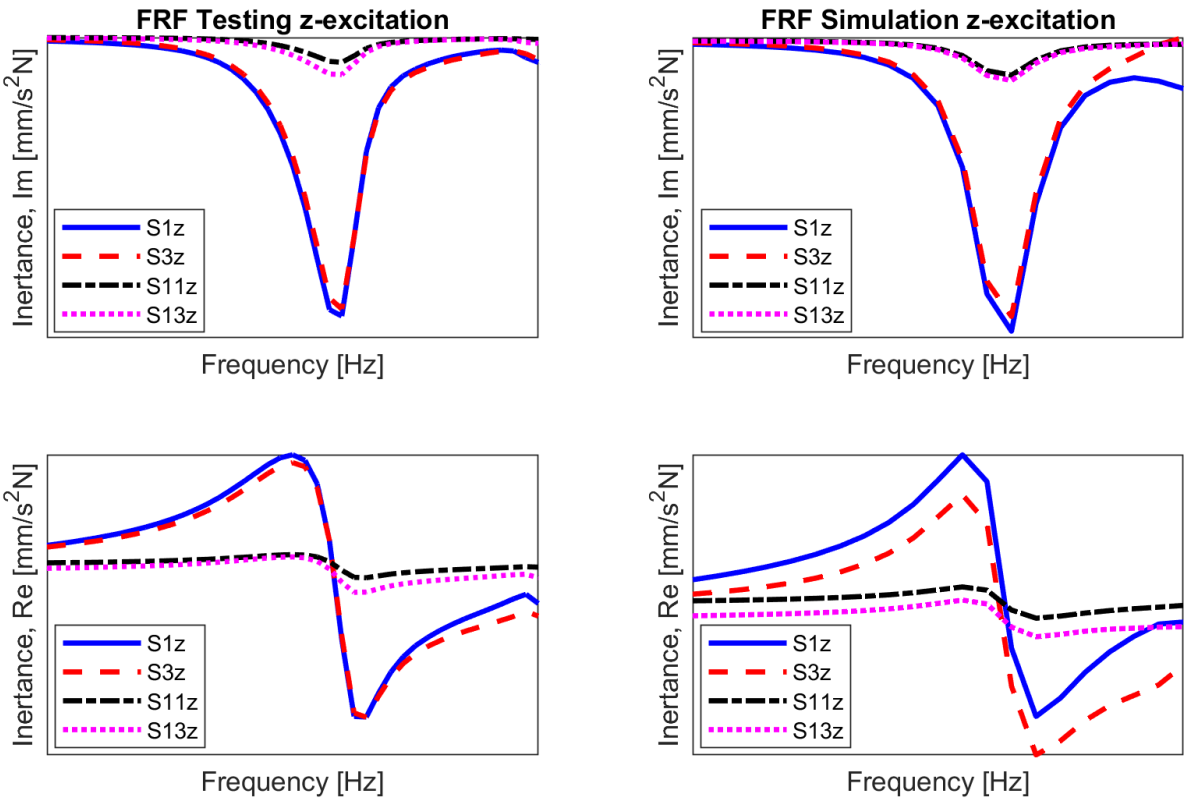

Figure 4.13. *Simulation and test results, real and imaginary part of inertance using z-response at three sensors. Global bending identified.*

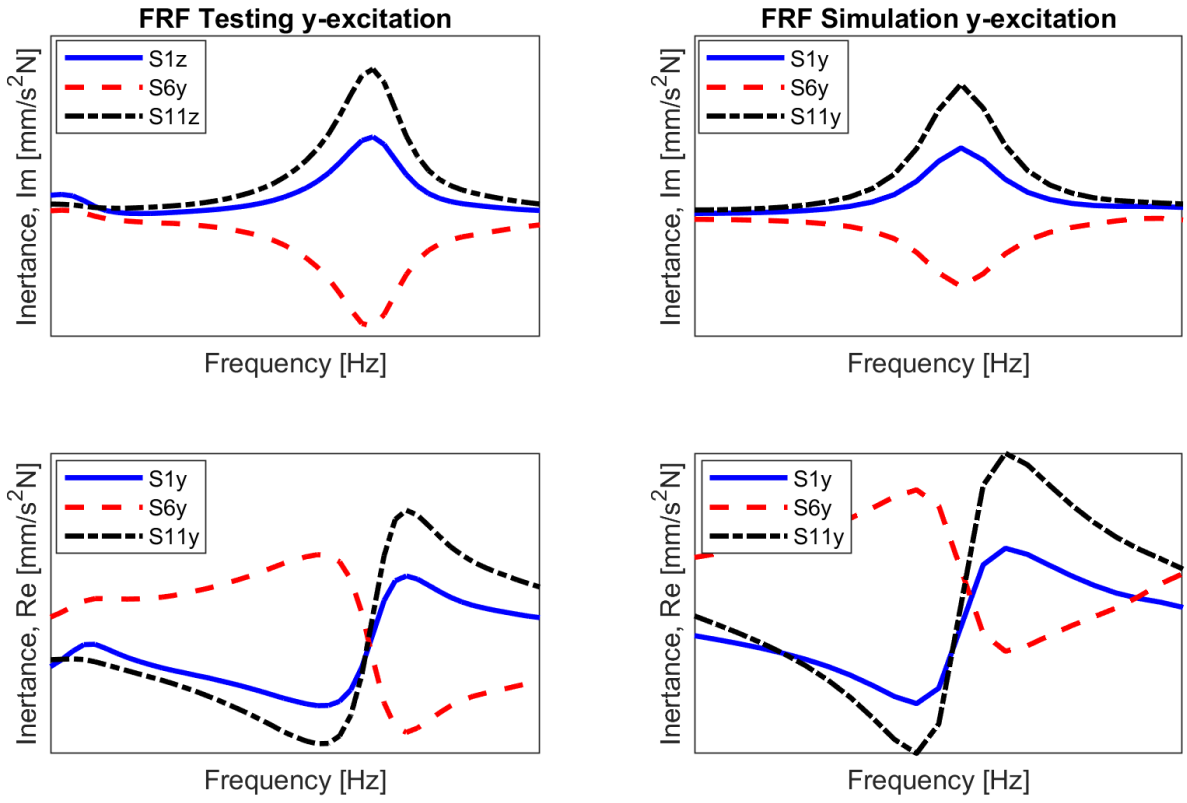

Figure 4.14. *Simulation and test results, real and imaginary part of inertance using z-response at three sensors. Lateral bending identified.*

4.7.2 Driving point FRFs

Once the correlation procedure has been completed drive point measurements can be plotted in the same figure for an easier overall comparison. In Figure 4.15, Figure 4.16, and Figure 4.17 this has been done for three different drive point measurements. The dotted line shows the simulation data before any adaptions were made regarding welds and adhesives to the current manufacturing step. The red line shows test data, whilst the blue line is an adapted FE-model to the current manufacturing step for the sub-assemblies.

As can be seen the CAE results on the Floor Rear are well correlated, also the magnitudes are on the same level because of the applied loss factor from measurement data. In the beginning of the studied frequency range, the analytical resonance frequencies are slightly overestimated, which can partly be explained by finite element theory. Since it can be proven that FE-models are always a stiffer version of reality, since the energy of the FE-solution is a lower bound of the energy of the exact solution (Larsson, personal communication, 31 March 2022). This holds true also for the Body Side Outer where the resonance frequencies were overestimated across the studied frequency range.

Higher in frequency range the overall correlation is worse, which can partly be explained by other uncertainties that have not been examined in this thesis. Two examples of uncertainties that could be studied further, are that some metal parts might be better modelled as orthotropic after metal forming, and that contact is not considered in this thesis.

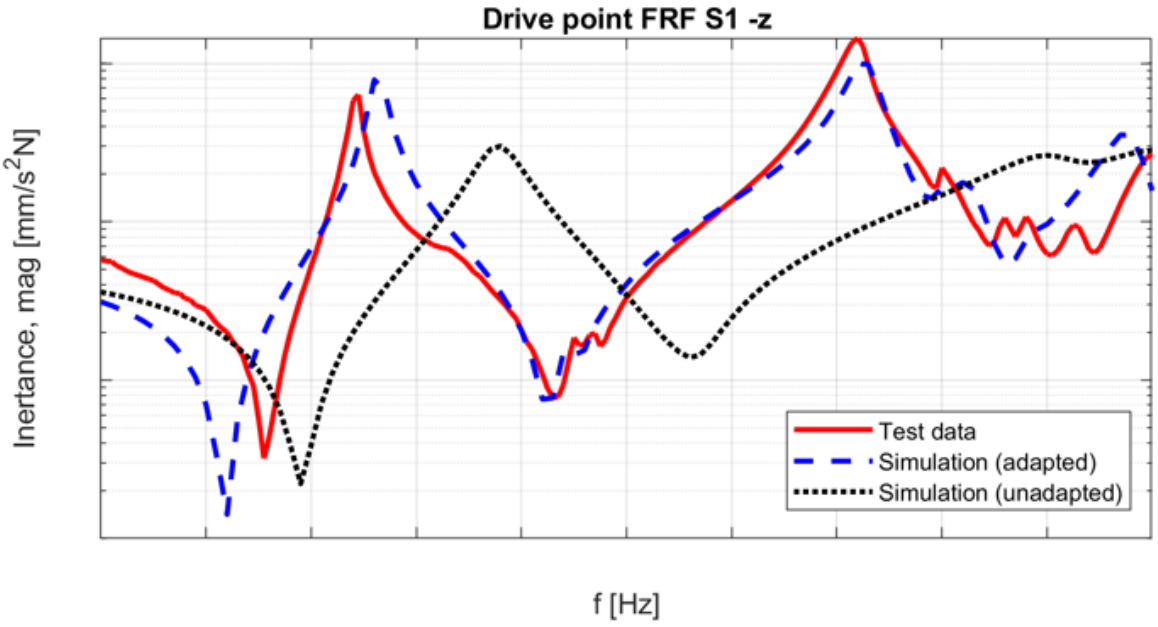

Figure 4.15. *Test data and simulation data compared in same window, drive point measurement* 1.

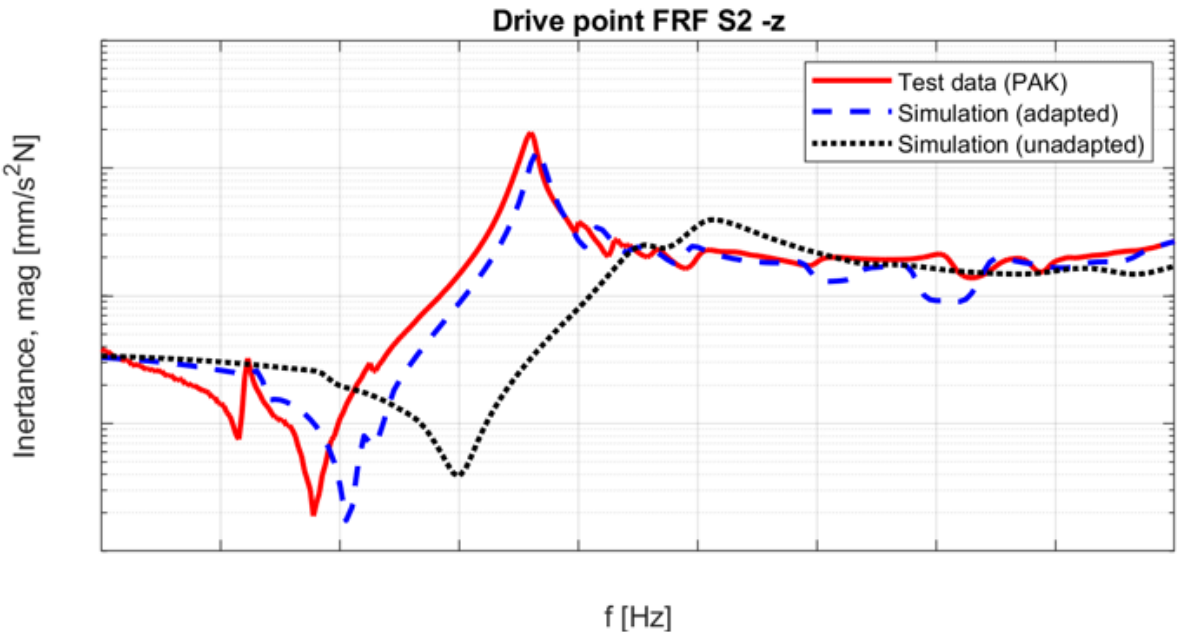

Figure 4.16. *Test data and simulation data compared in same window, drive point measurement* 2.

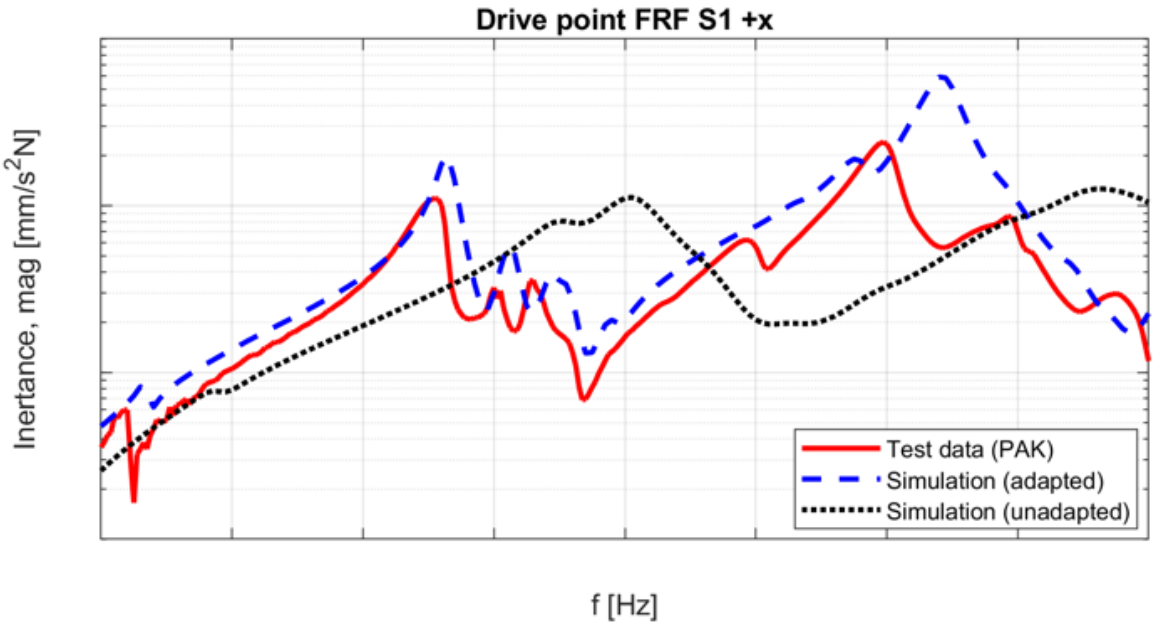

Figure 4.17. *Test data and simulation data compared in same window, drive point measurement* 3

4.7.3 Modal Assurance Criterion (MAC)

Once the correlation task is completed an accepted modal assurance correlation matrix should be obtained. Using the frequency response functions from measurements, the eigenvectors could be obtained directly from the peak amplitudes of the imaginary part of the transfer functions.

In Figure 4.18 below the co-linearity of eigenvectors is illustrated with black colors, and orthogonality by white. A well correlated model should, in addition to other criteria, have a diagonal with MAC-numbers close to 1, with a lower limit of around 0.95. For this dissertation these numbers ranged between 0.97 and 1 and thus the model can be considered validated in this sense. The first MAC-number presented in Figure 4.18 above was calculated using the eigenvectors obtained from the accelerance from simulation and measurement data respectively. The response was collected as the magnitude at the resonance frequencies, identified using the direct method. Below an example is given for the Global Torsion mode from a test where 9 accelerometers have been used.

$$\boldsymbol{\phi}_{iX}^{T} = [-1.0543 \quad -0.0469 \quad 0.9834 \quad -1.0098 \quad 1.0000 \quad -0.0226 \quad 0.9926 \quad -0.1344 \quad -0.9401]$$

$$\boldsymbol{\phi}_{jA}^{T} = [\,-0.9851 \quad 0.0101 \quad 1.0000 \quad -0.9330 \quad 0.9318 \quad -0.0018 \quad 0.8357 \quad 0.0101 \quad -0.7901]$$

$$MAC(i,j) = \frac{\left(\boldsymbol{\phi}_{iX}^{T}\boldsymbol{\phi}_{jA}\right)^{2}}{\|\boldsymbol{\phi}_{iX}\|_{2}^{\,2}\left\|\boldsymbol{\phi}_{jA}\right\|_{2}^{\,2}} = 0.99$$

The MAC matrix shows that the global modes have a similar mode shape in test and in CAE. Similar results were seen during the experimental modal analysis presented earlier when simulating the mode shapes from test and CAE.

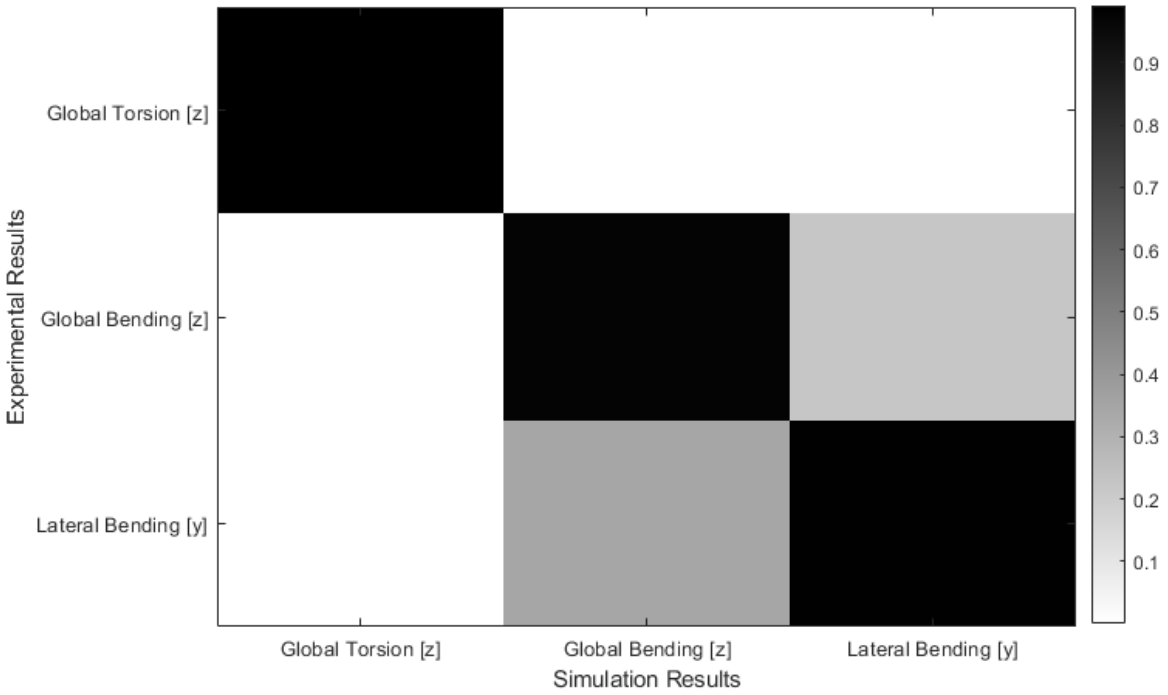

Figure 4.18. *MAC matrix illustrated with colors, co-linearity is indicated by black and complete orthogonality of eigenvectors by white.*

5. Conclusion

In Figure 4.4 it was concluded that the mass of the structure is already well correlated, with minor changes when adjusting the mass. This difference was further studied using metal forming simulations from LS-DYNA, implemented in the FE-model. It was then seen that the mass difference between measurements and NASTRAN output-files decreased rapidly by introducing forming simulations. However, the mass difference itself did not affect the eigenfrequencies or the mode shape in a noticeable way, especially lower in the studied frequency range.

Secondly the adhesives and welds were studied, here it was noticed that the sub-assembly correlation procedure proposed in this text requires several model changes. Both material data and connections are defined for the final complete vehicle and adapting these to the current step in the manufacturing requires extra procedures. This included using an overhead crane and lifting sling chains in the NVH-lab at VCC to be able to study the physical parts visually also beneath the structure for identification of weld nuggets.

It could be concluded that the hardening of the adhesives gives an increase of 2 % on the first studied eigenfrequency on the Floor Rear. Thus, if the same method is intended to be used also in upcoming work, it is important to study the current step in the process flow and adapt the FE-model after these differences. These results also give interesting insight in how much the adhesives contribute to the dynamical properties, and in which direction dynamical properties are affected. Furthermore, the welds decreased the first studied eigenfrequency with about 20% which suggests that results are highly sensitive to the joining of the different panels. Some spot welds are that added at a later stage in the manufacturing, which of course must be considered in simulation when correlating sub-assemblies as well.

Thirdly, the damping was studied on the Floor Rear as well as the Body Side Outer. Figure 4.9 shows the changes when updating the model with damping from measurements on the Floor Rear. This is also something to take into consideration when correlating sub-assemblies as in the proposed procedure in this dissertation. The damping decreases for the sub-assembly compared to the BIW. Thus, the damping cannot be applied from other FE-models but must be calculated from measurements individually for each sub-assembly and then applied in the FE-model.

The three steps above were looped, using the results presented in for example Figure 4.12, where the global modes were identified and the eigenfrequency determined for each iteration. During correlation the difference in eigenfrequency between test and CAE decreased as seen in Table 4.5.

To further improve the FE-model, a mapped thickness of the side-members was introduced in Figure 4.10. The frequency difference on the Global Torsion mode then decreased from 5% to about 3%, as well as improving the mass correlation to measured values. Thus, introducing more metal forming simulation results would give an overall higher accuracy of the results,

however only marginally compared to other uncertainties Here it was also noted that the strain energy density gives a good indicator on which parts a mapped thickness would affect most when introducing these in the FE-model.

Two different sets of boundary conditions were used during vibration testing, one of which imposed extra constraints to the structure compared to the previous suspension. The measurements showed that the first flexible mode then increased in frequency. Avitabile (2001) has shown that a difference of 5% in frequency can be seen also when a ratio of 10:1 is used for the flexible and rigid body modes. Thus, the difference when increasing the constraints of the supports is to be expected, and the results from the less stiff support should be used for correlation to mimic free-free conditions in simulation. This highlights some of the uncertainties in the test setup as well.

Lastly, the purpose of this master's thesis was fulfilled since several uncertainties could be localized using a smaller system than the complete body. Once the connections were adapted in ANSA for the current step in the manufacturing process, the FE-model had good correlation to test data. Introducing the damping was an important step as well, to highly increase the accuracy of the magnitudes of the transfer functions. The mapped thickness further improved the overall results and could be introduced if tougher requirements on the validation are used. The location and size of spot welds and weld lines should carefully be examined if well correlated results are of interest since they highly affect the dynamical properties of the structure.

6. Future Work

Two of the sub-assemblies have been correlated in this project with good results. Since the remaining sub-assemblies are connected and manufactured using the same techniques and similar tools, well correlated results are to be expected also on the excluded parts. The proposed future work is thus to correlate the complete BIW before and after the surface treatments, such as the electro-coating, as a final step without correlating the remaining sub-assemblies individually.

The modelling techniques used at VCC can thus be considered well developed, and the FE-models captures the modal properties seen from test data with high correlation. A proposed future work is thus to employ the proposed correlation methodology when a new concept is introduced, to ensure high correlation is achieved to test data also when the modelling guidelines have not been tested in this context before.

References

Abrahamsson, T. (2000). *Linear system theory in vibration engineering*. U72, Applied Mechanics, Chalmers.

Altair. (2022). *Altair Hypergraph – Comprehensive CAE Post-processing and Engineering Data Visualization*. Retrieved from: https://www.altair.com/hypergraph/. 2022-04-30.

ANSYS. (2022). *Ansys LS-DYNA Multiphysics Solver*. Ansys LS DYNA | Crash Simulation Software. 2022-03-31

Avitabile, P. (2001). Experimental Modal Analysis – *A Simple Non-Mathematical Overview*. Sound & Vibration magazine.

Böttcher, C., Frik, S. (2003). *Consideration of Manufacturing Effects to Improve Crash Simulation Accuracy*. 4th European LS-DYNA Users Conference. Ulm, Germany.

Craig, R. (2011). *Fundamentals of structural dynamics*. Wiley-Blackwell.

Dorendorf, G. (2017). *Variability of nominally identical components and their influence in an assembly - Applications to a Volvo XC90.* Chalmers University of Technology / Department of Mechanics and Maritime Sciences, Applied Mechanics. https://hdl.handle.net/20.500.12380/250365 . 2022-04-24.

Eppler, T., Schatz, R. (2007). *Modelling of spot welds for NVH simulations in view of refined* panel meshes. Chalmers University of Technology / Department of Civil and Environmental Engineering, Applied Acoustics. https://hdl.handle.net/20.500.12380/72499.

Fu, Zhi-Fang., He, Jimin. (2001). *Modal Analysis*. Elsevier Science & Technology.

(a) Hexagon. (2021). *MSC Nastran 2013 Design Sensitivity and Optimization User's Guide*. Retrieved from MSC Nastran 2013 Design Sensitivity and Optimization User's Guide (hexagon.com). 2022-03-17

(b) Hexagon. (2021). *MSC Nastran 2021.3 - Quick Reference Guide (PDF)*. Retrieved from MSC Nastran 2021.3 - Quick Reference Guide (PDF) (mscsoftware.com). 2022-03-16.

Hågeryd, L., Björklund, S., Lenner, M. (2016). *Modern Produktionsteknik Del 1*. Liber AB.

Mohanty, N. (1987). *Signal Processing*. Springer.

Müller-BBM VibroAkustik Systeme GmbH. 2022. *PAK 6.X*. Müller-BBM VibroAkustik Systeme: PAK 6.x (mbbm-vas.com). 2022-03-21.

Ottosen, N., Petersson, H. (1992). *Introduction to the finite element method*. Prentice Hall.

Siemens. (2022). *Simcenter Testlab*. Retrieved from https://www.plm.automation.siemens.com/global/en/products/simcenter/testlab.html. 2022-04-21.

Peeters, B., Guillaume, P., Van der Auweraer, H., Cauberghe, B., Verboven, P., Leuridan, J. (2004). *Automotive and aerospace applications of the PolyMAX modal parameter estimation method*. Proceedings of IMAC 22, the International Modal Analysis Conference.

DEPARTMENT OF MECHANICS AND MARITIME SCIENCES
CHALMERS UNIVERSITY OF TECHNOLOGY
Gothenburg, Sweden 2022
www.chalmers.se

CHALMERS
UNIVERSITY OF TECHNOLOGY